Large Scale Eigenvalue Calculations for Computing the Stability of Buoyancy Driven Flows

E. A. Burroughs[†‡], L. A. Romero[†], R. B. Lehoucq[†], and A. G. Salinger[†]

[†] *Sandia National Laboratories, Albuquerque N.M., 87185. Sandia is a multiprogram laboratory operated by Sandia Corporation, a Lockheed-Martin Company, for the United States Department of Energy under Contract DE-AC04-94AL85000*

[‡] *University of New Mexico, Albuquerque, N.M. 87131*

We present results for large scale linear stability analysis of buoyancy driven fluid flows using a parallel finite element CFD code (MPSalsa) along with a general purpose eigensolver (ARPACK). The goal of this paper is to examine both the capabilities and limitations of such an approach, with particular focus on solving large problems on massively parallel computers using iterative methods. We accomplish our goal by solving a large variety of two and three dimensional problems of varying difficulty, comparing our results (whenever possible) to semi-analytical results. We also carefully explain how we successfully combined Cayley transformations with an Arnoldi based eigensolver and preconditioned Krylov methods for the necessary linear solves.

For problems where the advective terms are not significant, we achieve excellent convergence of the computed eigenvalues as we refine the finite element mesh. We also successfully solve advectively dominated problems, but the convergence is slower. We believe that the main difficulties arise not from problems with the eigensolver, but from the accuracy of the finite element discretization. Therefore, we believe that our results are as reliable as using transient integration but are more efficiently computed. The largest eigenvalue problem we solve has over 16 million unknowns on 2048 processors.

Key Words: stability, Navier Stokes, eigenvalues, buoyancy driven flow, Arnoldi, bifurcation, finite element, massively parallel

1. INTRODUCTION

Much of our understanding of fluid flow phenomena comes from linearized stability analyses of simple flows, such as the state of rest, Couette flow, or Poiseuille flow [3, 22, 10, 18]. Modern computational fluid dynamicists routinely analyze the stability of more complicated flows using a variety of methods (e.g. spectral methods, boundary integral methods). However, the majority of these calculations are

done in such a way that the resulting linear systems can be solved using direct methods, and the calculations are typically done using codes that are tailored for the particular problem of interest [2, 41, 6].

In this paper we are concerned with the problem of combining a general purpose massively parallel finite element CFD code (MPSalsa [32]) with an existing Arnoldi based eigensolver (ARPACK [20]) and a parallel Krylov methods package (AZTEC [38]) for linearized stability analysis. MPSalsa discretizes the Navier-Stokes equations and applies Newton's method to solve for the steady state. This is in contrast to the standard approach of performing a transient calculation. While tried and true, this latter approach does not allow the computation of 'unstable steady states'. The former approach does detect unstable steady states thus allowing bifurcation analysis; the reader is referred to the recent review article [8] for further information along these lines.

The purpose of this paper is to explore the limits of our computational approach for linear stability analysis on a representative class of problems. For example, can we reliably determine the linear stability of a simple problem such as the Rayleigh-Bénard problem and for a more difficult problem such as turbulent transition in a boundary layer?

We carefully address the difficulty in the numerical solution of the eigenvalue problem and consider the sensitivity of the eigenvalues to discretization errors. We present a variety of problems of varying degrees of difficulty and show how our linearized stability analysis behaves on these problems. We validate our results by comparing the calculations to analytical solutions, highly resolved spectral calculations, or to published results involving time dependent numerical calculations. In addition, we verify our results via mesh refinement for the finite element discretization and by checking the residual accuracy of our computed eigenvalues and linear systems.

Because our interest is in discretized Navier-Stokes equations that lead to linear systems of order 10^4—10^7 for two and three dimensional problems, direct methods (let alone sparse direct methods) for the linear solves or subspace iteration for the eigensolve are not an option. We will demonstrate that parallel Krylov iterative methods can be reliably used for large-scale linear stability analysis on massively parallel machines.

We are not aware of any study comparable in scope to ours, that is, a comprehensive chronicle of the verification and validation of computational linear stability analysis utilizing parallel Krylov methods for complex fluid flow. We believe our approach to be as reliable as calculations accomplished with transient based methods. We believe our approach to be more efficient than transient based methods because we use a Krylov subspace method and use a frozen Jacobian and the non-linear convection solve made at every time step by a transient calculation is avoided. Moreover, our approach also provides qualitative information on the fluid flow not otherwise available. We believe that our approach is successful because we have employed the use of three existing robust and sophisticated tools: MPSalsa, ARPACK, and AZTEC.

We have chosen to concentrate on problems involving thermal convection. We anticipate that our examples will be of use to others interested in testing their codes' ability to do linearized stability analysis. We present results demonstrating

the success of our approach on a wide variety of problems. We do point out that our approach becomes computationally intensive as the fluid flow is more advectively dominated.

Advectively dominated flows are characterized by eigenvalues that typically have a large imaginary part relative to the real part. This results in two major difficulties. First, it can be difficult to compute the eigenvalues of the discretized system. For the problems presented in this paper, the use of a Cayley transformation along with an Arnoldi based algorithm proved sufficient. The second difficulty is that we may need to discretize the Navier-Stokes equations on a highly resolved mesh so that the real part of the eigenvalues will approximate those of the continuous system. We overcome this difficulty only by keeping the size of the linear systems within reason.

We divide our test problems into four basic groups:

1. Problems where the steady state solution has no flow or is a state of rigid body rotation. These problems include variants on the classical and the rotating Rayleigh-Bénard problem. We solve these problems in two and three dimensions and with different geometries and boundary conditions. We demonstrate excellent agreement between the computed eigenvalues and those using semi-analytical techniques. We acknowledge that these problems are easy to solve; we include them in this report for two reasons. First, they allow us to verify and validate our use of preconditioned Krylov methods, and second, they provide benchmarking data for others wishing to perform linearized stability analyses.

2. Problems where the steady state solution has flow, but the flow is not advectively dominated. We solve a variety of physically distinct problems: the onset of convection in a thermo-siphon, the onset of convection in a tilted two dimensional box, and the onset of convection in a tilted three dimensional box. In all of these problems the steady state solution whose stability we analyze has a non-zero velocity. But, in all cases this velocity is either small or contributes little to the heat transfer. We demonstrate convincingly that our code can handle problems of this type.

3. Problems where the steady state solution is advectively dominated. First, we consider the problem of flow in a two dimensional box with a heated side wall [28]. This differs from the flow in a heated slot only in the aspect ratio; however, the instability that occurs happens at a large value of the Grashoff number and is an oscillatory instability. We also analyze the problem of stability of a plume in a closed cylindrical container [36]. The performance of our code on these problems is somewhat disappointing in that we need fine meshes to accurately compute converged real parts of the eigenvalues of interest. We will show that this is due to discretization errors, not to a failure of the eigensolver to compute the correct eigenvalues. For this reason we believe a transient finite element code would have the same difficulty accurately computing these flows.

4. The bifurcation of steady state convection rolls into oscillatory convection rolls. In this problem the steady state solution has a significant flow that affects the heat transfer, but the flow is still not strongly advectively dominated. Due to the three dimensional nature of this problem and that we need to make the container large to remove the end effects of the side walls, it is difficult to get enough resolution to

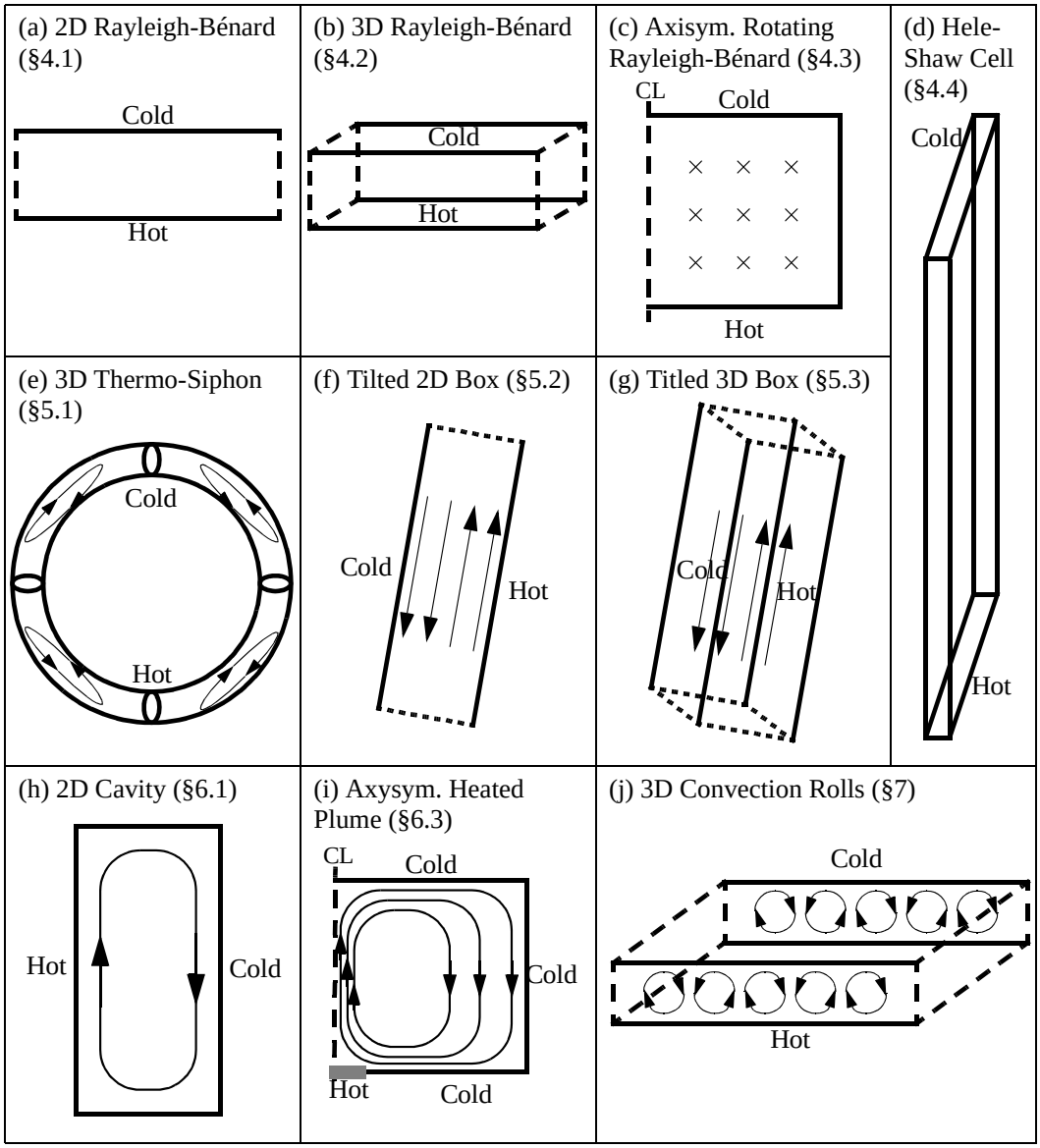

FIG. 1. Here we illustrate the ten problems considered in this paper. Solid lines represent no-slip boundary conditions, long dashed lines represent no tangential stress boundary conditions, and short dashed lines represent periodic boundary conditions. We indicate streamlines of the base flow.

convincingly solve this problem. We believe that we have just barely managed to resolve this problem; on our most highly refined grid over sixteen million unknowns were required for the discretization.

We will now outline the remainder of our report. In Section 2 we state the Navier-Stokes equations with the Boussinesq approximation governing the motion of all of the test problems in this paper. We discuss the possibility that mathematically equivalent but numerically different schemes for making our equations dimensionless

can behave differently. In Section 3 we discuss the finite element code MPSalsa. In Section 4 we discuss the Cayley transform, how to choose the Cayley parameters and the Arnoldi based eigenvalue package ARPACK. Section 5 presents the problems where the basic state is either at rest or uniformly rotating. Section 6 gives results for problems where the basic flow field is non-trivial, but not advectively dominated. Sections 7 and 8 give results for oscillatory convection in a slot, the instability of an axisymmetric confined plume, and the secondary bifurcation from steady rolls into oscillatory rolls in the Rayleigh-Bénard problem. In Section 9 we highlight some of the numerical difficulties that arise in the solution of these problems.

2. BASIC EQUATIONS AND THE EFFECT OF DIFFERENT SCALINGS

Throughout this paper we will be using the Navier-Stokes equations with the Boussinesq approximation for the flow of a thermally driven incompressible fluid:

$$\frac{\partial \mathbf{u}}{\partial t} + \mathbf{u}\cdot\nabla\mathbf{u} + \frac{1}{\rho}\nabla p = \nu\nabla^2\mathbf{u} + g\beta(T - T_{ref})\mathbf{e}_g \tag{1}$$

$$\frac{\partial T}{\partial t} + \mathbf{u}\cdot\nabla T = \kappa\nabla^2 T \tag{2}$$

$$\nabla\cdot\mathbf{u} = 0 \tag{3}$$

where $\mathbf{u} = u\mathbf{e}_x + v\mathbf{e}_y + w\mathbf{e}_z$, p and T are the velocity, pressure and temperature; ρ, ν and κ are the density, kinematic viscosity, and thermal diffusivity; g and β are the acceleration of gravity and the thermal expansion coefficient of the fluid. The vector $\mathbf{e}_g$ is a unit vector in the direction of the gravity vector. The Boussinesq approximation assumes that the temperatures T are all close enough to an average temperature T_{ref} that we can ignore the variations in density in all terms in the equations except for the forcing term due to gravity. In these equations we subtract the hydrostatic part of the pressure.

Other than the physical constants appearing in the equations, the only parameters appearing in the problems in this paper are the temperature difference ΔT, the characteristic geometrical length L, geometrical aspect ratios, and in one of the problems, the rotation rate Ω. In all of the problems considered the length L is the height or width of our container and $T_{ref} + \Delta T$ is the temperature on some part of the boundary. The other parts of the boundary either have no flux conditions or are at a temperature of T_{ref}.

The remainder of this section discusses the important issues of dimensionless parameters and the impact on scaling. Any dimensionless parameters that result from the physical parameters from the previous paragraph are functions of the Rayleigh number

$$Ra = \frac{g\beta\Delta T L^3}{\kappa\nu},$$

the Prandtl number

$$Pr = \frac{\nu}{\kappa},$$

the Taylor number

$$Ta = \frac{4R^4\Omega^2}{\nu^2},$$

and geometrical aspect ratios such as $\epsilon = R/L$ where R is the radius of a cylinder and L its height.

There are several standard ways of making our equations dimensionless. All these scalings can be implemented by setting the values of the dimensional variables equal to simple functions of the Rayleigh and Prandtl numbers within the code. In this paper we typically achieve the desired Rayleigh and Prandtl numbers by selecting $\nu = g = \beta = \rho = L = 1$, and $\kappa = 1/Pr$. We then control the Rayleigh number using $Ra = \Delta T Pr$.

There are two points we would like to make about our choice of scaling. The first point is that scaling changes the eigenvalues. This is not a numerical issue, but merely an issue of how to transform between different scalings. Our scaling uses the dimensionless time $\hat{t} = t/t_0$ where $t_0 = \frac{L^2}{\nu}$. We compute dimensionless eigenvalues λ. The physical eigenvalues $\lambda_{physical}$ are given by

$$\lambda_{physical} = \lambda \frac{\nu_{physical}}{L^2_{physical}}.$$

Here $\nu_{physical}$ and $L_{physical}$ are the physical values of ν and L, rather than the values used in our calculations (usually unity).

If a calculation is done using an alternative scaling that leads to identical values of the dimensionless constants, then the alternative eigenvalues are related by the expression

$$\lambda_{alt} = \lambda \frac{\nu_{alt}}{L^2_{alt}} \frac{L^2_{ours}}{\nu_{ours}},$$

where ν_{alt} and L_{alt} are the values of ν and L used in the alternative scaling, and ν_{ours} and L_{ours} are the values used in our calculation.

The second point about scaling deals with numerical issues. In theory our computed approximations to physical quantities should not depend on our choice of how to make the equations dimensionless, but in practice roundoff errors might reveal a sensitivity. Earlier versions of our linear solver demonstrated a sensitivity upon the scaling of the problem. For the simplest problem we present, the classical Rayleigh-Bénard problem in two dimensions, we found that a balanced scaling where $\nu = 1/Ra^{1/2}$ and $\Delta T = Ra^{1/2}$, achieved satisfactory results, but when we used $\nu = 1$ and $\Delta T = Ra$, no significant digits in the eigenvalues were computed when $Ra = 2000$. This sensitivity was traced to a use of a classical Gram-Schmidt algorithm needed by the GMRES algorithm used for the solution of the linear equations. The cure was to employ a two step classical Gram-Schmidt algorithm (the second step is to ensure orthogonality).

3. SPATIAL DISCRETIZATION AND THE NON-LINEAR SOLVE

A full description of the numerical methods in MPSalsa used to locate steady state solutions of Equations (1)—(3) is available in [32] and the references listed therein. A brief overview is presented in this section.

A mesh of quadrilaterals for 2D problems and hexahedra for 3D problems is generated to cover the domain. Although the code allows for general unstructured meshes, all the example problems in this paper use structured meshes. For parallel

runs, the mesh is partitioned using the Chaco code [14] in a way that will distribute work evenly while minimizing communication costs between processors. A Galerkin/least-squares finite element method [16] (GLS-FEM) is used to discretize the time-invariant versions of the governing partial differential equations (1)—(3) into a set of nonlinear algebraic equations. This formulation includes a pressure stabilization term so that the velocity components, temperature, and pressure fields can all be represented with equal order nodal basis functions. GLS-FEM is a consistent stabilized scheme because when the exact solution is inserted, the Boussinesq equations are satisfied exactly. We use bilinear and trilinear nodal elements for two and three dimensional problems, respectively.

Discretization of (1)—(3) results in the matrix equation

$$\begin{pmatrix} \mathbf{M} & \mathbf{0} \\ \mathbf{N} & \mathbf{0} \end{pmatrix} \begin{bmatrix} \dot{\mathbf{u}} \\ \dot{\mathbf{p}} \end{bmatrix} + \begin{pmatrix} \mathbf{K}_{u,T} + \mathbf{C}(\mathbf{u}) & -\mathbf{D} \\ \mathbf{D}^T + \mathbf{G} & \mathbf{K}_p \end{pmatrix} \begin{bmatrix} \mathbf{u} \\ \mathbf{p} \end{bmatrix} - \begin{bmatrix} \mathbf{g} \\ \mathbf{h} \end{bmatrix} = \begin{bmatrix} \mathbf{0} \\ \mathbf{0} \end{bmatrix} \tag{4}$$

where $\mathbf{u}$ is the vector of fluid velocity components and temperature unknowns, $\mathbf{p}$ is the pressure, $\mathbf{M}$ is the symmetric positive definite matrix of the overlaps of the finite element basis functions, $\mathbf{K}_{u,T}$ is the stiffness matrix associated with velocity and temperature, $\mathbf{C}(\mathbf{u})$ is the nonlinear convection, $\mathbf{D}$ is the discrete (weak) gradient, $\mathbf{D}^T$ is the discrete (weak) divergence operator, and $\mathbf{K}_p$ is the stiffness matrix for the pressure. $\mathbf{G}, \mathbf{K}_p, \mathbf{N}$ are stabilization terms arising from the GLS-FEM. The vectors $\mathbf{g}$ and $\mathbf{h}$ denote terms due to boundary conditions and the Boussinesq approximation.

The resulting nonlinear algebraic equations arising from setting the time derivative terms to zero are solved using a fully coupled Newton-Raphson method [33]. An analytic Jacobian matrix for the entire system is calculated and stored in a sparse matrix storage format. At each Newton-Raphson iteration, the linear system is solved using the Aztec package [38] of parallel preconditioned Krylov iterative solvers. The accuracy of the steady state solve is determined by

$$\left(\frac{1}{N} \sum_{i=1}^{N} \left(\frac{|\delta_i|}{\epsilon_R |x_i| + \epsilon_A} \right)^2 \right)^{\frac{1}{2}} < 1.0 \tag{5}$$

where ϵ_R and ϵ_A are the relative and absolute tolerances desired, δ_i is the update for the unknown x_i, and N is the total number of unknowns. We used relative and absolute tolerances of 10^{-5} and 10^{-8}, respectively, for the problems. We exclusively use an unrestarted GMRES iteration with a non-overlapping Schwarz preconditioner where an ILU preconditioner is used on each sub-domain (each processor contains one sub-domain). These methods enable rapid convergence to both stable and unstable steady state solutions. The scalability of these methods to large system sizes and numbers of processors is demonstrated by the solution of a 16 million unknown model on 2048 processors in Section 8.

4. THE DISCRETIZED EIGENVALUE PROBLEM AND CAYLEY TRANSFORMS

The GLS-FEM results in a spatial discretization of the Navier-Stokes equations with the Boussinesq approximation. This leads to a finite dimensional system of

differential algebraic equations of the form

$$\mathbf{B}\dot{\mathbf{x}} = \mathbf{F}(\mathbf{x}), \qquad \mathbf{x}(0) = \mathbf{x}_0, \tag{6}$$

where the matrix $\mathbf{B}$ is singular (due to the divergence free constraint) and $\mathbf{x}$ is a vector containing the values of the velocities, temperature and pressure at the nodes of the finite element mesh. Because of the stabilization terms in the GLS discretization, $\mathbf{B}$, the matrix associated with the time derivative term in (4), is a non-symmetric matrix.

Suppose we have a steady state solution $\mathbf{x}_s$ so that $\mathbf{F}(\mathbf{x}_s) = 0$. The stability of this solution is typically determined in one of two ways. The first approach solves the generalized eigenvalue problem

$$\lambda \mathbf{B}\mathbf{z} = \mathbf{J}(\mathbf{x}_s)\mathbf{z} \equiv \mathbf{J}\mathbf{z}. \tag{7}$$

that arises from the linearization of (6) about the steady state. The matrix $\mathbf{J}(\mathbf{x}_s)$ is the Jacobian of $\mathbf{F}(\cdot)$ linearized at $\mathbf{x}_s$. If all the eigenvalues of (7) have negative real parts, the steady state is stable. We assume that the λ's are ordered with respect to decreasing real part; $\text{real}(\lambda_j) \leq \text{real}(\lambda_i)$ for $i > j$.

This approach has received much attention in the last fifteen years; the reader is referred to [4, 7, 12, 26, 11, 21, 37, 39, 25] for information. Except for [39], all of these papers advocate converting the generalized eigenvalue problem (7) into a standard eigenvalue problem and then solving the resulting set of linear equations during each iteration of the eigensolver. Except for [11, 21, 37], the eigenvalue problem is solved using inverse subspace iteration or Arnoldi's method with a sparse direct method for the resulting linear set of equations. This typically limits the linear stability analysis to two dimensional problems. Our approach of using Cayley transformations to reduce (7) to a standard eigenvalue problem leads the authors of [12, p.1189] to state that all such "variants that we tested failed". The use of preconditioned Krylov methods for both the eigenvalue problem and ensuing linear solves for large-scale two and three dimensional problems is not generally undertaken. The results of our paper will show otherwise.

The second approach used to determine the stability of a steady state is to use a time integration scheme; standard time integration schemes typically perform a nonlinear solve (due to convection) at every time step. We can think of these as computing an iteration of the form

$$\mathbf{x}^{n+1} = \mathbf{G}(\mathbf{x}^n). \tag{8}$$

The iteration is initialized with an iterate near the steady state and if the iteration converges towards the fixed point $\mathbf{x}_s$, then the steady state is declared stable. If $\mathbf{x}_0$ is an initial condition for (8), then the convergence and numerical stability of the fixed point iteration is determined by the spectral radius of the Jacobian of $\mathbf{G}(\cdot)$. In particular, denote the eigenvalues of $\mathbf{G}_{\mathbf{x}}(\mathbf{x}_0)$ by γ_i ordered so that $|\gamma_j| \leq |\gamma_i|$ for $i > j$.

A popular time integration scheme is given by the trapezoidal rule and results in the iteration

$$\mathbf{x}^{n+1} = \mathbf{G}(\mathbf{x}^n) = \left(\mathbf{B} - \frac{\triangle t}{2}\mathbf{J}\right)^{-1}\left(\mathbf{B} + \frac{\triangle t}{2}\mathbf{J}\right)\mathbf{x}^n \tag{9}$$

where the Jacobian is 'frozen' at the steady state. The eigenvalues γ_i and λ_i are related via

$$\gamma_i = -\frac{\lambda_k + \frac{2}{\triangle t}}{\lambda_k - \frac{2}{\triangle t}} \quad i = 1, \ldots, n; k = 1, \ldots, n$$

and so, in principle, the eigenvalues of (7) can be determined by computing those of

$$-\left(\mathbf{J} - \sigma\mathbf{B}\right)^{-1}\left(\mathbf{J} - \mu\mathbf{B}\right)\mathbf{z} \equiv \mathbf{G}\mathbf{z} = -\gamma\mathbf{z}$$

where $\mu = -\sigma = 2/\triangle t$. The above discussion demonstrates that at a steady state, time integration and computing the eigenvalues of (7) are intimately related when a frozen Jacobian approximation is employed. We remark that although large-scale eigensolvers (subspace iteration or Arnoldi's method) applied to $\mathbf{G}$ tend to favor the computation of $\gamma_1, \gamma_2, \ldots, \gamma_r$—those largest in magnitude—these may not be the desired rightmost eigenvalues $\lambda_1, \ldots, \lambda_r$. This occurs, for instance, when the flow is advectively dominated.

We now explain why Arnoldi's method for the eigenvalue solvers is preferred to the typically undertaken transient calculation. A transient calculation (with the linearized Jacobian $\mathbf{J}$) or fixed point iteration is equivalent to the power method on $\mathbf{G}$. The rate of convergence to the eigenvector associated with γ_1 is $|\gamma_2/\gamma_1|$. The rate of convergence improves to $|\gamma_{m+1}/\gamma_1|$ if the power method is replaced by subspace iteration on m vectors. However, the resulting rate of convergence can be intolerable.

The rate of convergence to $\gamma_1, \gamma_2, \ldots, \gamma_r$ may be dramatically improved by projecting $\mathbf{G}$ onto the column space of

$$\mathbf{x}^0, \mathbf{x}^1, \cdots, \mathbf{x}^m.$$

Arnoldi's method [1] iteratively determines an orthogonal basis for the above column space that by definition is a Krylov subspace.

4.1. Arnoldi's method and the numerical solution of the eigenvalue problem

The remainder of the section reviews several issues with the use of Arnoldi's method for the numerical solution of the eigenvalue problem. We use the parallel implementation [23] P_ARPACK of ARPACK [20] for computing the eigenvalues of (7) via Cayley transformations. We refer the reader to [21] for information regarding the use of ARPACK for problems in linear stability analysis.

We discuss the selection of the Cayley parameters σ and μ. The numerical experiments that follow employ two strategies to select the Cayley parameters. The first strategy was presented in the previous subsection and draws upon a connection with fixed point iteration. The second strategy was presented in [21]; the Cayley parameters are selected $0 < \sigma < \mu$ so that the condition number of $(\mathbf{J} - \sigma\mathbf{B})^{-1}(\mathbf{J} - \mu\mathbf{B})$ is bounded and so can be efficiently solved with preconditioned Krylov methods. This second strategy is slightly more efficient than the first strategy; however, it is not as reliable (nor is there a relationship with fixed point iteration schemes for determining the stability of the steady state). The lack of reliability manifests itself when the flow is advectively dominated so that the rightmost λ's do not correspond

to the largest in magnitude γ's. We remark that we encountered this unreliability in the solution of the problem of the secondary bifurcation from steady rolls into oscillatory rolls in the Rayleigh-Bénard problem, discussed in section 8. Throughout the rest of the paper we will refer to the first strategy as Cayley Method A and the second as Cayley Method B.

We briefly overview several salient issues. The paper [21], section 9 and the discussion of the numerical experiments performed for each problem provide further details.

1. We discuss the numerical solution of the linear system resulting from using a Cayley transformation. We exclusively use an unrestarted GMRES iteration with a non-overlapping Schwarz preconditioner where an ILU preconditioner is used on each sub-domain (each processor contains one sub-domain).

2. We must choose the size of the Arnoldi space m (needed by ARPACK). Our findings, in general, are that for the most difficult problems m was never larger than 160 and 80 was typically more than adequate. We remark that although ARPACK does provide a capability to restart the Arnoldi iteration, our experiments did not use this capability. Instead, our focus is to carefully examine the use of preconditioned Krylov methods for linear stability analysis.

3. The tolerance needed by the GMRES iteration and ARPACK and their relationship was also carefully studied in [21]. In general, these tolerances were no larger than 10^{-6} and no smaller 10^{-9}.

4. Since the Boussinesq equations (1)–(3) model an incompressible fluid, the starting vector for ARPACK is selected as $\mathbf{J}^{-1}\mathbf{B}\mathbf{w}$, where $\mathbf{w}$ is a random vector. The resulting vector is divergence free [24].

5. The P_ARPACK subroutines `pdnaupd` and `pdneupd` were modified to implement the Cayley transformation and an improved check for termination. The eigensolve is terminated when $\lambda_1, \lambda_2, \ldots, \lambda_r$ and corresponding approximate eigenvectors for a user specified r satisfy the residual tolerance.

5. PROBLEMS WHERE THE FLUID IS AT REST OR IN UNIFORM ROTATION

In this section we present four problems where the base flow is either at rest or in a uniform state of rotation:

- The Rayleigh-Bénard problem in a two dimensional box.
- The Rayleigh-Bénard problem in a three dimensional box.
- The Rotating Rayleigh-Bénard problem in a cylinder.
- The Rayleigh-Bénard problem in a three dimensional box with two of the vertical side walls closely spaced (a Hele-Shaw cell).

The boundary conditions on the first three of these problems are chosen so that, in addition to the finite element solution, we can use the method of separation of variables to turn these higher dimensional eigenvalue problems into one dimensional eigenvalue problems that can be solved accurately. We use spectral collocation methods [13] to solve these one dimensional problems. We remark that the boundary conditions for these three problems are not physically realizable. The last

problem uses physically realizable boundary conditions, but we cannot use separation of variables to check our answers. Instead we validate our answers using an asymptotic expansion based on the analogy between a Hele-Shaw cell and a porous medium. We are then able to use the results for the onset of convection in a porous medium [42] to verify our calculations.

5.1. The Two Dimensional Rayleigh-Bénard Problem

We consider the Rayleigh-Bénard problem in two dimensions. Our geometry consists of a rectangular container of height H and length L:

$$0 \leq z \leq H, \;\; 0 \leq x \leq L.$$

We specify the temperature at the top and bottom surfaces

$$T(x,0) = T_{ref} + \Delta T \;\; , \;\; T(x,H) = T_{ref},$$

and specify that there is no flux of heat through the side walls

$$\frac{\partial}{\partial x} T(0,z) = \frac{\partial}{\partial x} T(L,z) = 0.$$

We have no-slip boundary conditions on the top and bottom walls

$$\mathbf{u}(x,0) = \mathbf{u}(x,H) = 0.$$

On the side walls we require that the normal velocity vanishes and that there is no tangential stress:

$$u(x,z) = \frac{\partial}{\partial x} w(x,z) \text{ for } x = 0, L.$$

This problem has the trivial solution

$$\mathbf{u} = 0$$

$$T(x,z) = T_{ref} - \Delta T (z - H)/H.$$

In Appendix A we show how to calculate the eigenvalues of the stability problem associated with this steady state solution using a one dimensional eigensolver.

We solve this problem in MPSalsa with $L = 3$, $H = 1$ and all physical parameters (g, β, ν, and κ) set equal to unity (in particular $Pr = 1$) except for ΔT, which is used to control the Rayleigh number. These calculations were done with N mesh divisions along the length of the rectangle and $2N$ mesh divisions along the height. The results for this problem are reported in Table 1. For the finest mesh, we have 116,644 unknowns and solve on 32 processors. We converge to the steady state easily given a zero initial guess. The number of GMRES solves for each eigensolver iteration is approximately 200. The time to compute eigenvalues on the finest mesh is 1374 seconds for Ra=2000. We use Cayley Method B and set the Cayley parameters $\sigma = 100$, $\mu = 1000$ and the Arnoldi size to 50. These results indicate

that we achieve quadratic convergence towards the exact eigenvalues; we compute convergence for a given eigenvalue as follows:

$$\text{Convergence Rate } = \log_2 \left(\frac{\lambda_{N/2} - \lambda_{analytic}}{\lambda_N - \lambda_{analytic}} \right).$$

Note for example that for $\lambda_0, Ra = 1500, N = 120$, the convergence rate is 2.32.

TABLE 1
The first 4 eigenvalues of the 2D Rayleigh-Bénard Problem with $L = 3$ and $H = 1$, Pr=1, $N \times 2N$ uniform mesh

Ra	N	λ_0	λ_1	λ_2	λ_3
1500					
	15	-1.898	-3.091	-5.151	-7.241
	30	-1.699	-3.088	-4.363	-7.251
	60	-1.652	-3.088	-4.178	-7.253
	120	-1.640	-3.088	-4.133	-7.254
	analytic	-1.637	-3.088	-4.118	-7.254
2000					
	15	1.913	-0.4021	-0.6466	-6.154
	30	2.100	0.1338	-0.4113	-6.046
	60	2.143	0.3146	-0.4141	-5.570
	120	2.153	0.3590	-0.4149	-5.454
	analytic	2.157	0.3738	-0.4151	-5.415

5.2. The Rayleigh-Bénard Problem in a Three-Dimensional Rectangular Box

We now add a third dimension and solve the problem on a rectangular box given by

$$0 \le x \le L, \;\; 0 \le y \le W, \;\; 0 \le z \le H.$$

Once again the boundary conditions on the side walls are chosen so that we can use separation of variables: the normal velocities, tangential stresses, and normal temperature gradients all vanish:

$$u(x,y,z) = \frac{\partial v(x,y,z)}{\partial x} = \frac{\partial w(x,y,z)}{\partial x} = \frac{\partial T(x,y,z)}{\partial x} = 0 \text{ for } x = 0, L$$

$$v(x,y,z) = \frac{\partial u(x,y,z)}{\partial y} = \frac{\partial w(x,y,z)}{\partial y} = \frac{\partial T(x,y,z)}{\partial y} = 0 \text{ for } y = 0, W.$$

As in the last section we prescribe no-slip boundary conditions on the horizontal walls and specify the temperature:

$$\mathbf{u}(x,y,z) = 0 \text{ for } z = 0, H$$

$$T(x,y,0) = T_{ref} + \Delta T, \;\; T(x,y,H) = T_{ref}.$$

For any value of the Rayleigh number this problem has the solution

$$\mathbf{u} = 0$$

$$T(x, y, z) = T_{ref} - (z - H)\Delta T/H.$$

In Appendix A we show how to calculate the eigenvalues of the stability problem associated with this steady state solution using a one dimensional eigensolver. Once again, we use a spectral collocation code to compute the eigenvalues of the one dimensional problem.

These calculations were done with MPSalsa on a box with $L = 3$, $H = 1$, $W = 1$, $g = \beta = \nu = \kappa = 1$, and $\Delta T = Ra$. The mesh has N divisions along the length L and width W, and $2N$ divisions along the height H. The results for this problem are reported in Table 2. For the finest mesh, we have 2,251,205 unknowns and solve on 512 processors. We converge to the steady state for $Ra = 500$ easily given a zero initial guess, then use continuation with steps of 500 to achieve the steady state at $Ra = 2000$. The number of GMRES solves for each eigensolver iteration is approximately 500. The time to compute eigenvalues on the finest mesh is 5817 seconds for Ra=2000. We use Cayley method B and set the Cayley parameters $\sigma = 10$, $\mu = 100$ and the Arnoldi size to 24. For the most part, we see quadratic convergence with mesh size; note that for $Ra = 1500$ the coarsest mesh does not show quadratic convergence, but as we refine the mesh we indeed see quadratic convergence. Note that for $\lambda_0, Ra = 1500, N = 60$, the convergence rate is 2.06.

TABLE 2
The first 4 eigenvalues of the 3D Rayleigh-Bénard Problem with $L = 3$, $H = 1$, $W = 1$, Pr=1, $N \times N \times 2N$ uniform mesh.

Ra	N	λ_0	λ_1	λ_2	λ_3
1500					
	15	-1.518	-1.663	-1.902	-2.614
	30	-1.612	-1.700	-1.738	-2.654
	60	-1.631	-1.652	-1.761	-2.665
	analytic	-1.637	-1.637	-1.769	-2.669
2000					
	15	2.376	2.233	1.909	1.665
	30	2.213	2.178	2.098	1.609
	60	2.166	2.162	2.148	1.596
	analytic	2.162	2.157	2.157	1.587

5.3. The Rotating Rayleigh-Bénard Problem

We now consider the problem of a fluid in a cylindrical container of radius R and height H whose axis is aligned with the direction of gravity. We use a 2D cylindrical coordinate system where the 3D vector (u, v, w) gives the radial, azimuthal, and axial components of the velocity. We rotate the cylinder about the axis of symmetry with a constant rotation rate Ω. Other than the change in geometry and the rotation, this problem is similar to the ones in the last two subsections.

In particular, on the top and bottom walls we impose no-slip boundary conditions and prescribe the temperature:

$$\mathbf{u}(r,z) = \Omega r \mathbf{e}_z \times \mathbf{e}_r \text{ for } z = 0, H \tag{10}$$

$$T(r,0) = T_{ref} + \Delta T, \;\; T(r,H) = T_{ref}. \tag{11}$$

In the first of these equations $\Omega r \mathbf{e}_z \times \mathbf{e}_r$ is the velocity of the container due to rotation. Note that in the classical analysis of this problem a Coriolis force is added to the equations of motion, but we impose the rotation through our boundary conditions.

Once again, the conditions on the side walls are chosen so that we can separate variables when solving the eigenvalue problem. We have no axial stress, no normal velocity, prescribed azimuthal velocity, and no flux conditions on the temperature:

$$u(r,z) = v(r,z) - r\Omega = \frac{\partial w(r,z)}{\partial r} = \frac{\partial T(r,z)}{\partial r} = 0 \text{ for } r = R. \tag{12}$$

This problem has an additional dimensionless parameter, the Taylor number:

$$Ta = \frac{4R^4\Omega^2}{\nu^2}.$$

This problem differs from the classical Rayleigh-Bénard problem in two respects [3]:

- For a given Taylor number, the critical Rayleigh number depends on the Prandtl number.
- If $Pr < 1$ we can have oscillatory instabilities.

This last point is what makes this an interesting test problem for our eigenvalue solver.

This problem always has the trivial solution where the fluid rotates like a rigid body and the temperature varies linearly with height:

$$u(r,z) = w(r,z) = 0$$

$$v(r,z) = r\Omega$$

$$T(r,z) = T_{ref} - \Delta T(z-H)/H.$$

In Appendix A we show how to calculate the eigenvalues of this steady state solution using a one dimensional eigensolver. We use a spectral collocation code to compute these eigenvalues.

In our numerical results we use $Pr = .025$ and $Ta = 1096.6$, resulting from $\nu = g = \beta = 1$, $\kappa = 40$, $R = 1$, and a rotation rate of $500rpm$. The calculations were done in cylindrical coordinates with N divisions in both the r and z directions. The results for this problem are reported in Table 3. For the finest mesh, we have 73,205 unknowns and solve on 32 processors. We converge to the steady state easily given a zero initial guess. The number of GMRES solves for each eigensolver

iteration is approximately 160. The time to compute eigenvalues on the finest mesh is 1014 seconds for Ra=4000. We use Cayley Method A and set the Cayley parameters $\sigma = 5$, $\mu = -5$ and the Arnoldi size to 50. Again, for the most part we see quadratic convergence with mesh refinement; note that the coarsest meshes for $Ra = 4000$ and $Ra = 5000$ show less than quadratic convergence, but as we refine the mesh we get quadratic convergence. Note that for the real part of $\lambda_0, Ra = 4000, N = 120$, the convergence rate is 2.17.

TABLE 3
The first 4 eigenvalues of the Rotating Rayleigh-Bénard Problem with $Ta = 4\Omega^2 R^4/\nu^2 = 1096.6$, $R/H = 1$, $Pr = .025$, $N \times N$ uniform mesh

Ra	N	λ_0	λ_1	λ_2	λ_3
4000					
	15	-10.5 ± 6.75 i	-36.0	-40.4	-76.8
	30	-8.25 ± 34.5 i	-35.3	-55.5 ± 7.48 i	-70.6
	60	-7.70 ± 39.7 i	-33.7	-54.5 ± 15.8 i	-68.2
	120	-7.56 ± 41.0 i	-33.2	-54.3 ± 17.4 i	-68.7
	analytic	-7.52 ± 41.5 i	-33.1	-54.2 ± 17.9 i	-68.0
5000					
	15	35.9	-18.9	-36.1	-40.9
	30	11.8	-9.33	-24.3	-35.7
	60	1.85 ± 17.4 i	-28.1	-34.0	-68.0
	120	1.98 ± 20.4 i	-29.3	-33.5	-66.3
	analytic	2.03 ± 21.3 i	-29.8	-33.4	-65.7

5.4. Convection in a Hele-Shaw Cell

In this subsection we consider the onset of convection cells in a three dimensional box with $0 \le x \le L$, $0 \le y \le W$, $0 \le z \le H$. We impose boundary conditions that are much easier to achieve experimentally: no-slip boundary conditions on all of the walls, no heat flux boundary conditions on the side walls, and prescribed temperatures on the horizontal walls:

$$\mathbf{u} = 0 \text{ on all walls}$$

$$T(x, y, 0) = T_{ref} + \Delta T, \quad T(x, y, H) = T_{ref}$$

$$\frac{\partial T}{\partial n} = 0 \text{ on all vertical walls.}$$

Once again this problem has the trivial solution where $\mathbf{u} = 0$ and $T = T_{ref} - \Delta T(z - H)/H$. We cannot analyze the stability of this problem using separation of variables, but if we assume that $W/H \ll 1$ and $W/L \ll 1$, we can approximate the eigenvalue problem accurately. The approximate equations are known as the Hele-Shaw cell approximation [31, p.123-125]. The resulting equations are identical to the equations for convection in a porous medium, which were analyzed in [42].

Assuming that the aspect ratio is small, then the pressure and temperature are nearly independent of y, there is almost no component of velocity in the y direction, and the velocities u and w vary quadratically with y. The approximate equations of motion can be written as

$$\mathbf{u}_{av} = \frac{k}{\mu}\left(\nabla p - \rho g \beta (T - T_{ref})\mathbf{e}_z\right) \tag{13a}$$

$$\left(\frac{\partial T}{\partial t} + \mathbf{u}_{av} \cdot \nabla T\right) = \kappa \nabla^2 T \tag{13b}$$

$$\nabla \cdot \mathbf{u}_{av} = 0. \tag{13c}$$

Here $\mathbf{u}_{av}(x, z)$ is the velocity averaged with respect to y. In these equations all quantities depend only on x and z, and all gradients and divergences are limited to x and z. In these equations the permeability k is given by

$$k = \frac{W^2}{12}. \tag{14}$$

The appropriate boundary conditions to impose are

$$u_{av}(x, z) = w_{av}(x, z) = 0 \text{ for } x = 0, L \text{ and } z = 0, H \tag{15}$$

$$\frac{\partial T(x, z)}{\partial x} = 0 \text{ for } x = 0, L \tag{16}$$

$$T(x, 0) = T_{ref} + \Delta T, \;\; T(x, H) = T_{ref}. \tag{17}$$

These equations are equivalent to those for two dimensional flow in a porous media. They asymptotically govern the motion of the fluid in the Hele-Shaw cell. They are the first term in an asymptotic expansion in the aspect ratio W/L where L is the characteristic dimension in the x and z directions. These equations also assume that Re_W, the Reynolds number based on W, is small. We emphasize that we do not solve these with the finite element code, but use these equations for validation of our results.

As with the fully three dimensional equations, these equations always have the trivial solution $\mathbf{u} = 0$, and $T(x, z) = T_{ref} + \Delta T(z - H)/H$. The stability of this steady solution depends on the Rayleigh number, Ra_{HS}, defined as

$$Ra_{HS} = \frac{\Delta T g \beta k H}{\kappa \nu} = \frac{\Delta T g \beta W^2 H}{12 \kappa \nu}.$$

In Appendix B we show how to analyze the stability of this no flow solution by using separation of variables. The resulting one dimensional eigenvalue problem is then solved using a spectral collocation method.

In the finite element code, we set $L = 1$, $H = 1$ and control the aspect ratio $\epsilon = W/H$ by changing W. We set $g = \beta = \kappa = \nu = 1.0$ and control Ra_{HS} with ΔT. In these results there are N mesh divisions along the width W and $2N$ along the length L and height H. The results for this problem are reported in Tables 4

and 5. For the finest mesh, we have 176,505 unknowns and solve on 64 processors. We converge to the steady state for $Ra_{HS} = 20$ using a zero initial guess, then use 3 continuation steps to achieve the steady state at $Ra_{HS} = 40$. The number of GMRES solves for each eigensolver iteration is approximately 600. The time to compute eigenvalues on the finest mesh is 3906 seconds for Ra=20 and $\epsilon = 0.05$. We use Cayley Method B and set the Cayley parameters $\sigma = 10$, $\mu = 100$ and the Arnoldi size to 24.

Though in this case we have asymptotic results as opposed to exact results, the difference between successive approximations tends towards a quadratic ratio.

TABLE 4
The first four eigenvalues of the Hele Shaw Cell with aspect ratio $\epsilon = 1/20$, $Pr = 1.0$, $N \times 2N \times 2N$ uniform mesh

Ra_{HS}	N	λ_0	λ_1	λ_2	λ_3
20					
	5	-9.927	-9.996	-37.269	-40.705
	10	-9.898	-10.112	-35.198	-39.794
	20	-9.875	-10.303	-34.630	-39.565
	asymptotic	-9.739	-9.870	-33.348	-39.478
30					
	5	-4.982	-9.916	-30.499	-40.669
	10	-5.275	-9.899	-27.966	-39.801
	20	-5.593	-9.882	-27.269	-39.558
	asymptotic	-4.739	-9.870	-25.348	-39.478
40					
	5	0.0685	-9.911	-23.714	-40.621
	10	-0.436	-9.886	-20.741	-39.781
	20	-0.884	-9.841	-19.891	-39.547
	asymptotic	0.261	-9.870	-17.348	-39.478

6. PROBLEMS WITH SMALL BUT NON-TRIVIAL BASE FLOWS

In this section we present results for problems where the base flow has non-zero velocity but is not strongly advectively dominated. We present three test problems: the onset of convection in a thermo-siphon, the onset of convection in a two dimensional tilted slot, and the onset of convection in a three dimensional tilted slot.

6.1. The Onset of Convection in a Thermo-Siphon

We now consider the stability of the flow in a closed loop thermo-siphon—a tube with a circular cross section of radius R_T that has been bent into a torus of radius R_H. The hoop walls are held at a prescribed temperature, where the temperature on the bottom of the hoop is hotter than that at the top.

Although the finite element calculations are done in Cartesian coordinates, the problem can best be formulated in terms of cylindrical coordinates (r, z, θ) with the

TABLE 5
The first four eigenvalues of the Hele Shaw Cell on a $N \times 2N \times 2N$ uniform mesh with $N = 20$, $Pr = 1.0$.

Ra_{HS}	ϵ	λ_0	λ_1	λ_2	λ_3
20					
	.1	-9.875	-11.053	-35.785	-39.560
	.05	-9.875	-10.303	-34.630	-39.565
	$\frac{1}{\infty}$	-9.739	-9.870	-33.348	-39.478
30					
	.1	-6.734	-9.869	-29.048	-39.554
	.05	-5.593	-9.882	-27.269	-39.558
	$\frac{1}{\infty}$	-4.739	-9.870	-25.348	-39.478
40					
	.1	-2.433	-9.870	-22.365	-39.551
	.05	-0.884	-9.841	-19.891	-39.547
	$\frac{1}{\infty}$	0.261	-9.870	-17.348	-39.478

position $\mathbf{x}$ given by

$$\mathbf{x}(r, z, \theta) = r\mathbf{e}_r + z\mathbf{e}_z \tag{18}$$

with

$$\mathbf{e}_z = (0, 0, 1) \tag{19}$$

$$\mathbf{e}_r = (\sin(\theta), \cos(\theta), 0) \tag{20}$$

$$\mathbf{e}_\theta = (\cos(\theta), -\sin(\theta), 0)\,. \tag{21}$$

The velocity vectors are defined as

$$\mathbf{u} = u\mathbf{e}_r + v\mathbf{e}_\theta + w\mathbf{e}_z. \tag{22}$$

In this coordinate system, the midline of the hoop is given by $r = R_H$, and each cross section with $\theta = constant$ is a circle of radius R_T. In other words, the tube is described by the equation

$$(r - R_h)^2 + z^2 \leq R_T^2.$$

We apply no-slip boundary conditions everywhere on the tube and prescribe the temperature on the boundary:

$$\mathbf{u}(r, z, \theta) = 0 \text{ on boundary} \tag{23}$$

$$T(r, z, \theta) = T_{ref} + \Delta T f(\theta) \text{ on boundary.} \tag{24}$$

Here $f(\theta)$ is a function that gives the temperature on the boundary as a function of θ; we use functions $f(\theta)$ that are even functions of θ.

Assuming that $R_T \ll R_H$, when the temperature difference is small there will be a small buoyancy-driven velocity field that is symmetric with respect to θ. However, when ΔT reaches a critical value, this symmetric state goes unstable, and the fluid will start circulating in one direction or the other. This problem cannot be reduced to a one dimensional eigenvalue problem. However, assuming that the radius of the tube is small compared to the radius of the hoop ($R_T \ll R_H$), we can solve this problem asymptotically. In Appendix C we present an asymptotic analysis for computing the eigenvalues for this problem.

The analysis in the Appendix shows that provided the aspect ratio $\epsilon = R_T/R_H$ is small enough, the stability of the symmetrical solution is governed by the parameter Ra_{therm} where

$$Ra_{therm} = \frac{g\beta R_T^4 A}{\kappa\nu R_H}\ , \tag{25}$$

and

$$A = \frac{\Delta T}{2\pi}\int_{-\pi}^{\pi} f(\theta)\cos(\theta)d\theta. \tag{26}$$

We have carried out the asymptotic analysis for the most unstable eigenvalue of the thermo-siphon problem and have compared it with the results of the most unstable eigenvalue computed using the finite element code. In MPSalsa we set $g = \beta = \kappa = \nu = 1$ and $f(\theta) = \cos(\theta)$. The mesh has $\frac{N}{4}$ by $\frac{N}{4}$ mesh divisions around a cross-section and $N + \frac{N}{20}$ mesh divisions about the circumference of the loop. The results are reported in Table 6. For the finest mesh, we have 185,220 unknowns and solve on 64 processors. We converge to the steady state easily using a zero initial guess. The number of GMRES solves for each eigensolver iteration is approximately 240. The time to compute eigenvalues on the finest mesh is 2671 seconds for Ra=30. We use Cayley Method B and set the Cayley parameters $\sigma = 10$, $\mu = 80$ and the Arnoldi size to 48. We see that once N is large enough, we get excellent agreement between the asymptotic and numerical results. This is a confirmation of both the numerics and the asymptotics.

TABLE 6
The first eigenvalue of flow in a thermo-siphon with $R_T = 1$, $R_H = 10$, $Pr = 1.0$, $\frac{N^2}{16} \times (N + \frac{N}{20})$ uniform mesh

N	$Ra_{therm} = 30$	$Ra_{therm} = 32.5$	$Ra_{therm} = 35$	$Ra_{therm} = 37.5$
20	-0.758	-0.533	-0.316	-0.108
40	-0.389	-0.163	0.054	0.264
80	-0.303	-0.078	0.139	0.348
asymptotic	-0.306	-0.082	0.133	0.341

6.2. The Onset of Convection Rolls in a Tilted Two Dimensional Box

In this subsection we discuss the onset of convection in a two dimensional tilted slot. When the tilt angle is 0, this is the classical Rayleigh-Bénard problem with

periodic boundary conditions at the vertical walls. When the tilt angle is 90 degrees, this is the problem of a slot with one vertical wall cooled and the other vertical wall heated. Periodic boundary conditions are imposed on the horizontal walls (so that the problem can be reduced to a one dimensional eigenvalue problem that is once again solved using the method of separation of variables). For any value of the tilt angle or Rayleigh number there is a trivial solution where the flow is unidirectional, going up the hot wall and down the cold wall. The temperature profile associated with this base flow is the same as if there were no flow at all.

We consider the equations for a Boussinesq fluid in a two dimensional rectangular box

$$0 \leq x \leq L, \quad -H/2 \leq z \leq H/2$$

with the gravity vector inclined with an angle θ relative to the z axis:

$$\mathbf{e}_g = \cos(\theta)\mathbf{e}_z - \sin(\theta)\mathbf{e}_x.$$

Physically this arises from tilting the box, but it is mathematically convenient to think of tilting the gravity vector.

We impose no-slip conditions on the walls with $z = constant$

$$\mathbf{u}(x, z) = 0 \text{ for } z = \pm H/2$$

and Neumann boundary conditions on the temperature

$$T(x, z) = \mp \Delta T/2 \text{ for } z = \pm H/2.$$

On the walls with $x = constant$ we impose periodic boundary conditions:

$$T(0, z) = T(L, z), \quad \mathbf{u}(0, z) = \mathbf{u}(L, z), \quad p(0, z) = p(L, z).$$

Assuming that we choose the reference temperature T_{ref} in the Boussinesq equations to be zero, we always have the simple solution

$$T_0(x, z) = -\frac{z\Delta T}{H} \tag{27a}$$

$$u_0(x, z) = -\frac{g\beta\Delta T \sin(\theta)}{6\nu H}\left(z^3 - \frac{H^2}{4}z\right) \tag{27b}$$

$$w_0(x, z) = 0 \tag{27c}$$

$$p_0(x, z) = -\frac{\rho g\beta\Delta T \cos(\theta)}{2H}z^2. \tag{27d}$$

Note that there is no net transport of mass across any plane $x = constant$ and that although the velocity does not vanish, the temperature profile is always the same as the conduction temperature profile. When $\theta = 0$ there is no flow, and we get the classical Rayleigh-Bénard problem. When $\theta = \pi/2$, we have the flow in a slot that is heated on one vertical wall and cooled on the other.

In Appendix D we show how to calculate the eigenvalues of the stability problem associated with this simple solution using a one dimensional eigensolver.

In MPSalsa we set $g = \beta = \kappa = \nu = 1$ and control the Rayleigh number with ΔT. The mesh has N divisions along the length L and $\frac{2N}{3}$ along the height H. We report our results in Table 7. For the finest mesh, we have 38,800 unknowns and solve on 8 processors. We converge to the steady state for $Ra = 7000$ easily using a zero initial guess, then use continuation steps of size 1000 to achieve the steady state at $Ra = 9000$. The number of GMRES solves for each eigensolver iteration is approximately 400. The time to compute eigenvalues for the finest mesh is 1904 seconds for Ra=7000 and $\theta = 80$ deg. We use Cayley Method B and set the Cayley parameters $\sigma = 10$, $\mu = 100$ and the Arnoldi size to 24. Note that the semi-analytical results predict that the eigenvalues are real, but have multiplicity two. The multiplicity of the eigenvalues arises because we are using periodic boundary conditions, and any eigenvalue associated with the spatial dependence e^{ikx} is also an eigenvalue of a mode with spatial dependence e^{-ikx}. For some values of Rayleigh number the results of the eigenvalue calculations show small residual imaginary parts instead of multiple eigenvalues, but we claim that these imaginary parts are small enough that they can be ignored.

TABLE 7
The first 4 eigenvalues of the tilted 2D box $L = 3$, $H = 1$, $Pr = 1.0$, $N \times \frac{2N}{3}$ uniform mesh .

Ra	θ	N	λ_0	λ_1	λ_2	λ_3
7000	90					
		30	-9.883 + 0.007 i	-9.883 - 0.007 i	-12.231	-12.231
		60	-9.875 + 0.017 i	-9.875 - 0.017 i	-12.244	-12.244
		120	-9.871 + 0.001 i	-9.871 - 0.001 i	-12.269	-12.269
		analytic	-9.870	-9.870	-12.286	-12.286
9000	90					
		30	0.525	0.525	-9.879	-9.886
		60	0.618	0.618	-9.863	-9.887
		120	0.638	0.638	-9.857	-9.885
		analytic	0.638	0.638	-9.870	-9.870
7000	80					
		30	-9.882 + 0.009 i	-9.882 - 0.009 i	-9.968	-9.968
		60	-9.875 + 0.015 i	-9.875 - 0.015 i	-10.017	-10.017
		120	-9.751	-10.050 + 0.011 i	-10.050 - 0.011 i	-10.586
		analytic	-9.870	-9.870	-10.100	-10.100
9000	80					
		30	2.422	2.422	-9.881	-9.883
		60	2.483	2.483	-9.875 + .005 i	-9.875 - .005 i
		120	2.486	2.485	-9.871 + .027 i	-9.871 - .027 i
		analytic	2.464	2.464	-9.870	-9.870

6.3. The Onset of Convection Rolls in a Tilted Three Dimensional Box

In this subsection we discuss the onset of convection in a three dimensional box that has been tilted so that the gravity vector still lies in one of the planes of symmetry. This is the same as the previous problem, but we have added a third dimension which we will call y. The boundary conditions in the third dimension are like those of the classical Rayleigh-Bénard problem presented in the last section. We are able to use separation of variables to compute modes that either have no y dependence or no x dependence. When the tilt angle is small the most unstable mode corresponds to rolls lining up with their axes aligned perpendicular to the axis of tilt. When the tilt angle is large, the rolls line up with their axis parallel to the tilt axis.

Once again we assume that the gravity vector is inclined at an angle θ to the z axis:

$$\mathbf{e}_g = \cos(\theta)\mathbf{e}_z - \sin(\theta)\mathbf{e}_x.$$

We consider convection in a three dimensional box

$$0 \leq x \leq L_x, \;\; 0 \leq y \leq L_y, \;\; -H/2 \leq z \leq H/2.$$

We impose no-slip boundary conditions on the planes $z = constant$

$$\mathbf{u} = 0 \text{ for } z = \pm H/2$$

and impose the temperature boundary conditions

$$T(x, y, z) = - \mp \Delta T/2 \text{ for } z = \pm H/2.$$

On the walls with $x = constant$ we impose periodic boundary conditions

$$T(0, y, z) = T(L_x, y, z), \;\; \mathbf{u}(0, y, z) = \mathbf{u}(L_x, y, z), \;\; p(0, y, z) = p(L_x, y, z).$$

On the walls with $y = constant$ we impose the conditions

$$\frac{\partial T}{\partial y}(x, y, z) = 0 \text{ for } y = 0, L_y$$

$$v(x, y, z) = 0 \text{ for } y = 0, L_y$$

$$\frac{\partial u}{\partial y}(x, y, z) = \frac{\partial w}{\partial y}(x, y, z) = \frac{\partial T}{\partial y}(x, y, z) = 0 \text{ for } y = 0, L_y.$$

We can use the method of separation of variables to find eigenvalues associated with modes that have no x dependence or modes that have no y dependence. There are modes that we cannot find using separation of variables; we indicate these in the tables by "miss." In MPSalsa we set $g = \beta = \kappa = \nu = 1$ and control the Rayleigh number with ΔT. The mesh has N divisions along the length L, $\frac{N}{3}$ along the width W, and $\frac{2N}{3}$ along the height H. The results for this problem are reported in Table 8. For the finest mesh, we have 1,992,600 unknowns and solve on 128

processors. We converge to the steady state for the lowest Rayleigh number using a zero initial guess, then use continuation steps of size 1000 to achieve the steady states for the higher Rayleigh numbers. The number of GMRES solves for each eigensolver iteration is approximately 500. The time to compute eigenvalues on the finest mesh is 5.7 hours for Ra=9000 and $\theta = 80\,\text{deg}$. We use Cayley Method B and set the Cayley parameters $\sigma = 10$, $\mu = 100$ and the Arnoldi size to 24.

TABLE 8
The first 4 eigenvalues of the tilted 3D box with $L = 3$, $H = 1$, $Pr = 1.0$, $N \times \frac{N}{3} \times \frac{2N}{3}$ uniform mesh.

Ra	θ	N	λ_0	λ_1	λ_2	λ_3
1500	10					
		30	-1.709	-2.919	-2.919	-3.362
		60	-1.791	-2.995	-2.995	-3.443
		120	-1.813	-3.017	-3.017	-3.464
		analytic	-1.822	miss	miss	-3.472
2000	10					
		30	2.092	1.251	1.251	-0.821
		60	1.981	1.150	1.150	-0.794
		120	1.952	1.123	1.123	-0.781
		analytic	1.939	miss	miss	-0.777
8000	80					
		30	-2.471	-3.635	-3.636	$-9.888 \pm 0.191i$
		60	-2.503	-3.492	-3.494	-9.839
		120	-2.520	-3.505	-3.507	$-9.871 \pm 0.084i$
		analytic	-2.550	-3.534	-3.534	-9.870
9000	80					
		30	$2.272 + 0.001i$	$2.272 - 0.001i$	-1.049	-9.751
		60	2.480	2.479	-1.081	-9.875
		120	2.487	2.485	-1.100	-9.813
		analytic	2.464	2.464	-1.132	-9.870

7. ADVECTIVELY DOMINATED FLOWS

In this section we present two problems where the flow is advectively dominated. The stability of these flows cannot be analyzed using separation of variables; we verify the accuracy of our results through comparison to previous numerical solutions and convergence as we refine the mesh. In both of these problems the imaginary parts of the eigenvalues are large, and we have slow convergence towards the real parts of the most unstable eigenvalue.

We believe that these problems demonstrate the limitations of what can robustly be done by applying a general purpose finite element code to a fluid stability calculation. However, we note that the difficulties are with the resolution of the discretization and not in solving the eigenvalue problem. We emphasize that a transient solution is not any more reliable than the eigenvalue computations. We also note that both of these problems are two dimensional; if we were trying to

achieve the same resolution on a three dimensional problem, we would have billions of unknowns.

7.1. The Onset of Oscillatory Convection in a Cavity

In this section we consider the problem of convection in a two dimensional vertical cavity of width W and height H

$$-W/2 \leq x \leq W/2$$

$$-H/2 \leq z \leq H/2.$$

This problem is almost identical to one studied by Paolucci and Chenoweth [28]. More recent work on this problem can also be found: see [17, 43, 15, 19, 44, 29]. In [28] they found oscillatory solutions using time dependent calculations. Here we will use eigenvalue calculations to predict the onset of oscillations.

The left vertical wall is held at a constant temperature $-\Delta T/2$, and the right vertical wall is held at the temperature $\Delta T/2$:

$$T(\pm W/2, z) = \pm \Delta T/2$$

We impose no flux boundary conditions at the horizontal walls

$$\frac{\partial T(x, \pm H/2)}{\partial z} = 0$$

and no-slip boundary conditions on all walls

$$\mathbf{u} = 0 \text{ on all walls.}$$

Paolucci and Chenoweth carried out their calculations with $Pr = .71$. Our calculations are carried out with $\nu = g = \beta = 1$, and $\kappa = 1/Pr = 1.0/.71$. The Rayleigh number is controlled using $Ra = \Delta T Pr$. We use $H = 2$ and $W = 1$.

In [28] they show that as the Rayleigh number is increased (based on the ΔT and W) boundary layers develop on both vertical walls, and "hydraulic jumps" develop at the upper left and lower right corners. The "hydraulic jump" in the upper left hand corner is where the flow moving up the left hand wall turns the corner and flows over a region of more dense fluid near the upper wall. A similar situation exists in the lower right hand corner. For $1/2 < H/W < 3$ they found that these "hydraulic jumps" would start oscillating at a Rayleigh number lower than that necessary to get the thermal boundary layers to go unstable. (Their explanation of the instability in terms of these "hydraulic jumps" is in dispute; see [17], for example.) This section is devoted to analyzing the onset of this oscillatory behavior using eigenvalue calculations.

Although Paolucci and Chenoweth did not make the Boussinesq approximation in their calculations, they purposely used conditions that are well approximated by the Boussinesq approximation. In particular, $\Delta T/T_{AV} = .01$ where ΔT is the difference between the wall temperatures and T_{AV} is the average of the wall temperatures. When $A = H/W = 2$ they found an instability at a Rayleigh number of approximately $Ra = 3 \times 10^7$ with a dimensionless frequency of $f = 173.2$.

Paolucci and Chenoweth use a dimensionless time based on the thermal conductivity, whereas we we use a dimensionless time based on the kinematic viscosity. Thus, we need to divide their frequencies by the Prandtl number to compare them to our frequencies. If f_{PC} are the frequencies reported in [28], then to get our frequencies ω_{ours} we use

$$\omega_{ours} = f_{PC}\frac{2\pi}{.71}$$

We use grids of 60×60, 120×120, 240×240 and 480×480. The spacing between the grid points increases exponentially as we move away from the walls, with the grids in the middle of the box having grid spacings about 20 times as large as the grids near the walls.

For the finest mesh, we have 925,444 unknowns and solve on 64 processors. It is somewhat difficult to achieve convergence of the steady state solution; we rely on continuation to find the steady state at the desired Rayleigh numbers. The number of GMRES solves for each eigensolver iteration is approximately 400. The time to compute eigenvalues for the finest mesh is 7 hours for $Ra = 3.0\times 10^7$. We use Cayley Method A and set the Cayley parameters $\sigma = 2000$, $\mu = -2000$ and the Arnoldi size to 160.

Table 9 shows the eigenvalues for the 240×240 grid and how they compare with the results of Paolucci and Chenoweth. Paolucci and Chenoweth only performed calculations at Rayleigh numbers of 3×10^7 and 2×10^7 for $A = 2.0$. The frequency they report at $Ra = 3\times 10^7$ is in excellent agreement with the frequency predicted by our eigenvalue calculation. However when $Ra = 2\times 10^7$ the frequency they report agrees with what we calculate to be the third most unstable mode. Furthermore, they report the flow as being stable, while the eigenvalue calculations report that the flow is unstable. Since we are close to the point of instability it is possible that their calculations are just slightly under-resolved.

In order to see how the steady state solution is converging with mesh refinement we have included Table 10. This table shows the maximum value of the radial velocity and its r and z location. We are clearly getting convergence, but the convergence with mesh is somewhat slow and clearly is no better than the convergence with mesh of the eigenvalues.

TABLE 9
The Eigenvalues for the convection in a cavity problem with mesh $N = 240$. Note that f_1 & f_2 are the frequencies reported by [28] and are only available for comparison for the two Rayleigh numbers 3.0×10^7 and 2.0×10^7

$Ra(10^7)$	$\Delta T(10^7)$	f_1	f_2	λ_0	λ_1	λ_2
3.0	4.225	1531.		468.2 ± 1546i	463.3 ± 1549i	-101.7 ± 4044i
2.75	3.873			383.7 ± 1488i	377.8 ± 1491i	-97.80 ± 3875i
2.5	3.521			283.1 ± 1424i	275.9 ± 1426i	-94.31 ± 3695i
2.25	3.169			164.7 ± 1352i	155.9 ± 1356i	-92.82 ± 3500i
2.0	2.817		3261.	35.86 ± 1262i	20.13 ± 1278i	-95.87 ± 3290i
1.5	2.113			-237.8 ± 982.5i	-156.3 ± 1035i	-199.7 ± 3148i

TABLE 10
Eigenvalues and maximum computed values for the radial velocity in the problem of the onset of oscillatory convection in a heated slot with $Ra = 3.0 \times 10^7$ with varying mesh resolution.

N	λ_0	λ_1	λ_2	r velocity	r-coord	z-coord
60	$460.0 \pm 1423i$	$457.2 \pm 1421i$	$-127.9 \pm 3951i$	1199.3	0.1232	0.9629
120	$475.5 \pm 1540i$	$471.0 \pm 1543i$	$-104.1 \pm 4038i$	1130.2	0.1203	0.9644
240	$468.2 \pm 1546i$	$463.3 \pm 1549i$	$-101.7 \pm 4044i$	1128.9	0.1224	0.9674
480	$467.7 \pm 1547i$	$462.4 \pm 1560i$	$-102.0 \pm 4045i$	1130.6	0.1216	0.9667

7.2. Comments on the symmetry and near-degeneracy of the eigenvalues

One interesting feature of these eigenvalue calculations is that we have two complex conjugate pairs of eigenvalues that are nearly identical. These eigenvalues are close enough that one might expect that they should be the same; from the symmetry of the problem we can argue that they are not the same. If the right vertical wall is held at a temperature that is the negative of the left vertical wall, then the governing equations are invariant under the following symmetry transformations:

$$Rz(\mathbf{x}) = \begin{pmatrix} -T(-\mathbf{x}) \\ -\mathbf{u}(-\mathbf{x}) \\ p(-\mathbf{x}) \end{pmatrix}$$

where we are representing our solution in the shorthand form

$$z(\mathbf{x}) = \begin{pmatrix} T(\mathbf{x}) \\ \mathbf{u}(\mathbf{x}) \\ p(\mathbf{x}) \end{pmatrix}.$$

If the functions $(T(\mathbf{x}), \mathbf{u}(\mathbf{x}), p(\mathbf{x}))$ satisfy the equations of motion and boundary conditions, then so do the functions $(-T(-\mathbf{x}), -\mathbf{u}(-\mathbf{x}), p(-\mathbf{x}))$, or put another way, if $z(\mathbf{x})$ is a solution to our equations, then so is $Rz(\mathbf{x})$. However, it is not necessary that solutions to our equations satisfy $Rz(\mathbf{x}) = z(\mathbf{x})$. Symmetry can only be broken through a bifurcation: a solution that is initially symmetric will stay symmetric as we vary a parameter unless we encounter a bifurcation point.

We are analyzing the stability of symmetric solutions; for this reason, all eigenfunctions will either be symmetric or anti-symmetric: any simple eigenfunction will either satisfy $R\phi(\mathbf{x}) = \phi(\mathbf{x})$, or $R\phi(\mathbf{x}) = -\phi(\mathbf{x})$.

We conclude that when our system goes unstable, the "hydraulic jumps" will either oscillate in a symmetric manner, or in an anti-symmetric manner. Physically we expect that if the walls are well separated, then the jump on the left should be able to oscillate independently of the jump on the right. In order for this to be so, we would have to be able to construct eigenfunctions where the jump on the left oscillates but the one on the right does not. The only way to do this is if we have multiple eigenvalues, with one eigenvector being symmetric, and the other one being anti-symmetric. This is not quite what occurs because the two jumps

do know a little bit about each other, but we almost get this. Hence we have two eigenvalues that are almost identical to each other.

7.3. The Stability of a Heated Plume

In this section we consider the problem of convection in a cylindrical container that has a hot spot on the bottom of the container. This problem was previously considered by Torrance and Rockett [36], who did a numerical and experimental study of the flow.

Let R be the radius of the container, H be the height, and R_s be the radius of the hot spot.

We define the aspect ratio as

$$\epsilon = \frac{H}{R}$$

and the spot aspect ratio as

$$\epsilon_s = \frac{R_s}{R}.$$

The problem of interest has no-slip boundary conditions on all walls

$$\mathbf{u} = 0 \text{ on all walls}$$

and specifies that the temperature is T_{ref} on all walls except on the hot spot, where it is $T_{ref} + \Delta T$:

$$T(r, 0) = T_{ref} + \Delta T \text{ for } r < R_s$$

$$T(r, 0) = T_{ref} \text{ for } R_s < r < R$$

$$T(r, H) = T_{ref} \text{ for } 0 < r < R$$

$$T(R, z) = T_{ref} \text{ for } 0 < z < H.$$

For compatibility with the previous work, we present results in terms of the Grashoff number, defined as

$$Gr = RaPr$$

As in [36] we use $\epsilon = H/R = 1$, and $\epsilon_s = R_s/R = .1$, and $Pr = \frac{1}{1.4}$. In our calculations we set $R = H = 1$, $R_s = .1$, $\nu = .01$, $\kappa = .014$, $g = 100$ and $\beta = 1$. We then control the Grashoff number using $Gr = \Delta T \times 10^6$.

In [36] they state that experimentally the flow was found to turbulent when

$$Gr > 1.2 \times 10^9.$$

Their numerical calculations assumed axisymmetry so were stable past the point of experimentally observed transition. They found that oscillations started occurring in the axisymmetric flows for Gr somewhere between 4×10^9 and 4×10^{10}.

Our calculations indicate that there is an unstable eigenvalue for $Gr > 1.0 \times 10^9$. Our calculations were carried out using $2N$ points in the vertical direction and N in the radial direction. In Table 11 we present the results for the most unstable eigenvalue with $Gr = 1.0 \times 10^9$ and different values of N; we used values of

$N = 40, 80, 160, 320$ and 640. The imaginary part of the most unstable eigenvalue appears to be converging quite rapidly as we refine the mesh. However, the convergence of the real part is somewhat disappointing. Table 11 shows that the slow convergence of the eigenvalues is a result of the slow convergence of the steady state as one refines the mesh.

For the finest mesh we have 3,284,484 unknowns and solve on 512 processors. It is somewhat difficult to achieve convergence of the steady state solution; we rely on continuation to find the steady state at the desired Grashoff numbers. The number of GMRES solves for each eigensolver iteration is approximately 320. The time to compute eigenvalues for the finest mesh is 2.9 hours for $Gr = 1.0 \times 10^9$. We use Cayley Method A and set the Cayley parameters $\sigma = 1200$, $\mu = -1200$ and the Arnoldi size to 160.

TABLE 11
The real and imaginary parts of the most unstable eigenvalue and maximum computed values for the radial velocity for the problem of a confined heated plume for $Gr = 1. \times 10^9$.

N	$Re(\lambda_0)$	$Im(\lambda_0)$	r velocity	r-coord	z-coord
40	155.1	$\pm$ 616.6	96.952	0.075	0.987
80	-4.898	$\pm$ 883.7	143.09	0.050	0.994
160	-14.24	$\pm$ 1109.	180.53	0.037	0.997
320	22.55	$\pm$ 1128.	163.52	0.037	0.997
640	36.70	$\pm$ 1130.	163.69	0.033	0.997

8. THE OSCILLATORY INSTABILITY OF CONVECTION ROLLS

In this section we present the results for a secondary bifurcation in the Rayleigh-Bénard problem. In particular we compute the convection rolls arising from the first bifurcation in the Rayleigh-Bénard problem; we then analyze the stability of these rolls. We have chosen our parameters so that we get an oscillatory instability. The stability of the rolls has been considered both experimentally [40] and numerically [2, 5, 35, 27, 34, 9].

In their paper Busse and Clever [2] numerically analyzed the stability of the convection rolls in the absence of any side walls. Their equilibrium solution is a two dimensional solution periodic in the direction perpendicular to the axis of the rolls. They analyze the stability of this solution by Fourier transforming the disturbances and looking for the most unstable wavelength. Their results show that as the Prandtl number goes to zero, the rolls have an oscillatory instability at a Rayleigh number close to the critical Rayleigh number of the first bifurcation. Although their results are in qualitative agreement with experiments, quantitatively their results predict the bifurcation occurs closer to the original bifurcation than the experiments do. They argue that this is most likely a result of ignoring the side walls.

We compute the stability of the convection rolls including the effect of the side walls. We assume that the flow takes place in a three dimensional box

$$0 \le z \le H, \;\; 0 \le x \le L, \;\; 0 \le y \le W.$$

In our calculations we choose $H = 1$, $L = W = 5$. We have tried to choose the aspect ratios L/H and W/H large enough that the effect of the side walls is not overwhelming, but small enough that we can resolve the rolls with a reasonable number of unknowns.

We prescribe the temperature on the horizontal walls

$$T(x, y, 0) = T_{ref} + \Delta T, \;\; T(x, y, H) = T_{ref},$$

and no flux boundary conditions on all side walls

$$\frac{\partial T}{\partial x}(0, y, z) = \frac{\partial T}{\partial x}(L, y, z) = \frac{\partial T}{\partial y}(x, 0, z) = \frac{\partial T}{\partial y}(x, W, z) = 0.$$

We prescribe no-slip boundary conditions at the horizontal walls and at the walls $x = constant$:

$$\mathbf{u}(x, y, 0) = \mathbf{u}(x, y, H) = \mathbf{u}(0, y, z) = \mathbf{u}(L, y, z) = 0.$$

At the walls $y = constant$ we prescribe no normal velocity, and no tangential stress:

$$v(x, 0, z) = v(x, W, z) = 0$$

$$\frac{\partial u}{\partial y}(x, 0, z) = \frac{\partial u}{\partial y}(x, W, z) = \frac{\partial w}{\partial y}(x, 0, z) = \frac{\partial w}{\partial y}(x, W, z).$$

We use a Prandtl number of $Pr = .01$. We achieve our dimensionless parameters using $g = \beta = \nu = 1$, $\kappa = 1/Pr = 100$, and $Ra = \Delta T/100$. Our mesh has N divisions in the L and W directions and $\frac{2N}{5}$ in the H direction. We report our results in Table 12. In Table 13 we report the maximum x-velocity and z-velocity and the z-coordinates at which they occur. Note that we see quadratic convergence in the velocities and their coordinates (taking into account the symmetry of the flow), indicating our mesh is fine enough to resolve the flow.

For the finest mesh, we have 16,362,405 unknowns and solve on 2048 processors. It is difficult to converge to the steady state for this problem for the fine mesh; we rely on continuation and mesh sequencing — that is, we use our solution from the coarser mesh and interpolate it to a solution on the finer mesh as an initial guess. The number of GMRES solves for each eigensolver iteration is approximately 375. The time to compute eigenvalues for the finest mesh is 9.5 hours for Ra=1850. We use Cayley Method A and set the Cayley parameters $\sigma = 60$, $\mu = -60$ and the Arnoldi size to 60. Here we note that choosing the Cayley parameters so that $0 < \sigma < \mu$ (Cayley Method B) is unreliable in that we do not converge to the complex conjugate pair that identifies the oscillatory instability; for example using $\sigma = 100$ and $\mu = 1000$ does not find this instability.

9. NUMERICAL ISSUES

TABLE 12
The first 4 eigenvalues of the Convection Rolls with $L = 5$, $W = 5$, $H = 1$, $Pr = .01$, $N \times N \times \frac{2N}{5}$ uniform mesh.

Ra	N	λ_0	λ_1	λ_2	λ_3
1850					
	50	-1.514	-3.725	-3.873	-4.222
	100	-3.059	-3.109	-3.810	-4.198
	200	-2.961	-3.360	-3.743	-4.111 $\pm$ 52.91 i
1900					
	50	-1.552	-3.064	-3.414 $\pm$ 59.82 i	-4.934
	100	-1.258 $\pm$ 71.84 i	-3.116 $\pm$ 85.87 i	-3.580 $\pm$ 54.86 i	-3.796
	200	-0.798 $\pm$ 74.30 i	-2.644 $\pm$ 88.80 i	-3.240 $\pm$ 56.74 i	-3.582
1950					
	50	-1.322 $\pm$ 74.34 i	-1.494	-2.488	-3.030 $\pm$ 88.94 i
	100	1.960 $\pm$ 94.33 i	0.541 $\pm$ 113.0 i	-1.38 $\pm$ 71.54 i	-4.53
	200	2.744 $\pm$ 99.06 i	1.428 $\pm$ 118.67 i	-0.814 $\pm$ 75.09 i	-4.236
2000					
	50	0.748 $\pm$ 89.41 i	-0.659 $\pm$ 107.1 i	-1.419	-2.139
	100	5.202 $\pm$ 119.1 i	4.662 $\pm$ 143.0 i	0.7943 $\pm$ 89.71 i	-1.806 $\pm$ 129.3 i

TABLE 13
Maximum computed values for variables in the Convection Rolls with $L = 5$, $W = 5$, $H = 1$, $Pr = .01$.

Ra	N	x vel	z-coord	y vel	z-coord
1850					
	50	50.7	0.8	44.9	0.55
	100	57.8	0.175	50.4	0.525
	200	59.1	0.8125	51.3	0.5125
1900					
	50	66.3	0.8	58.1	0.5
	100	80.0	.175	70.3	0.525
	200	82.9	0.825	73.0	0.5125
1950					
	50	82.4	0.8	73.5	0.5
	100	104.5	0.175	93.5	0.5
	200	109.7	0.175	98.5	0.5
2000					
	50	98.8	0.8	89.7	0.5
	100	130.6	0.175	119.2	0.5

Because we use parallel preconditioned Krylov iterative methods for the eigenvalue problem and resulting linear sets of equations, our results are obtained by specifying the values of certain adjustable parameters. For example, we needed to specify the Cayley parameters σ and μ and the size of the Arnoldi space. We briefly review our verification procedures used for all the numerical experiments;

the reader is referred to [21] for further information. Our main emphasis in this section is to illustrate how sensitive our results are to the Cayley parameters.

Denote by λ_c and $\mathbf{z}_c$ the approximations to an eigenvalue and eigenvector of (7). We verify these approximations by computing the norm of the residual

$$\frac{||\mathbf{J}\mathbf{z}_c - \lambda_c \mathbf{B}\mathbf{z}_c||}{||\mathbf{B}\mathbf{z}_c||}, \tag{28}$$

and the Rayleigh quotient error

$$|\lambda_c - \frac{\mathbf{z}_c^H \mathbf{J}\mathbf{z}_c}{\mathbf{z}_c^H \mathbf{B}\mathbf{z}_c}|, \tag{29}$$

where $||\cdot||$ is the Euclidean norm of a vector and $\mathbf{z}^H$ denotes the conjugate transpose of a vector. These errors only vanish when λ_c and $\mathbf{z}_c$ are an eigenpair for (7). Note that these measures are independent of the scaling of $\mathbf{z}_c$ and ARPACK scales the approximate eigenvector so that $\|\mathbf{z}\| = 1$.

We now discuss the Cayley parameters and the size m of the Arnoldi space used by ARPACK. These two parameters are related because if one chooses the Cayley parameters poorly, a large Arnoldi space will be required to obtain accurate eigenvalues. Our experience dictates that it is best to choose the Cayley parameters so that they are on the order of magnitude of the imaginary part of the most unstable eigenvalue. We believe that this is a reasonable assumption because the user typically has some idea of the location of the imaginary part of the most unstable eigenvalue. For example, this information is available if we are solving a problem that is a small variation of a problem that has already been solved, or if we have access to related experimental or computational results. However, this is a drawback because some idea of the size of the imaginary portion of the most unstable eigenvalue is required. Our experience is that for some of the problems, our estimate could be off by several orders of magnitude and not affect the computation. On other problems we observed degraded performance when we were off by a factor of two in choosing the Cayley parameters. None of the problems we solved show extreme sensitivity to the choice of the Cayley parameters.

We use the problems of oscillatory convection in a slot and the stability of a heated plume as illustrations of the effect of these parameters. On physical grounds it is difficult to predict that one of these problems would be more sensitive to our choice of Cayley parameters than the other. However, the problem of the onset of convection in a slot is considerably less sensitive to our choice of Cayley parameters than the problem of the instability of the plume.

Table 14 shows the errors in the most unstable eigenvalue of the onset of convection in a heated slot as a function of the Cayley parameters and the size of the Arnoldi space. These calculations were accomplished with a 120×120 mesh, and a Rayleigh number of 1.5×10^7. We see that changing the Cayley parameters from ± 1000 to ± 250 does not significantly degrade the performance of the algorithm. By the time the Cayley parameters are ± 50 we are seeing some degradation in the algorithm, but we are still getting quite good convergence after 160 iterations.

Table 15 shows the same results for the problem of the stability of a heated plume. Here we are using the 160×320 grid with a Grashoff number of 1×10^9.

The results for an Arnoldi space of 80, and Cayley parameters of ± 250 are clearly inferior to those for the same size Arnoldi space but Cayley parameters of ± 1000.

The accuracy of all of these calculations is limited by the accuracy to which we solve our linear systems. For example, in Table 15 we do not get appreciably better results by using an Arnoldi space of size 160 instead of 80. A discussion of the effect of our linear algebra tolerances on the eigenvalues is given in [21].

TABLE 14
The effect of Arnoldi size and Cayley parameters on the problem of convection in a heated slot. These results are for the most unstable eigenvalue at $Ra = 1.5 \times 10^7$, and a grid of 120×120.

$\sigma = -\mu$	Arnoldi Size	Eigenvalue (normalized by 10^{-2})	Direct Residual	Rayleigh Quotient
50				
	20	-2.022 ± 10.30 i	5.351 $\times 10^{1}$	2.167
	40	-1.429 ± 10.43 i	7.956	6.270 $\times 10^{-1}$
	80	-1.411 ± 10.40 i	1.252$\times 10^{-3}$	4.199 $\times 10^{-5}$
	160	-1.411 ± 10.40 i	1.252 $\times 10^{-3}$	4.199 $\times 10^{-5}$
125				
	20	-2.132 ± 10.27 i	5.193 $\times 10^{1}$	5.888
	40	-1.417 ± 10.40 i	5.689	2.920 $\times 10^{-1}$
	80	-1.411 ± 10.40 i	5.689 $\times 10^{-4}$	3.240 $\times 10^{-5}$
	160	-1.411 ± 10.40 i	5.689 $\times 10^{-4}$	3.240 $\times 10^{-5}$
250				
	20	-2.031 ± 10.31 i	1.496 $\times 10^{2}$	1.095 $\times 10^{1}$
	40	-1.412 ± 10.40 i	2.513	8.351 $\times 10^{-2}$
	80	-1.411 ± 10.40 i	2.438 $\times 10^{-4}$	2.871 $\times 10^{-6}$
	160	-1.411 ± 10.40 i	2.438 $\times 10^{-4}$	2.871 $\times 10^{-6}$
500				
	20	-1.259 ± 10.83 i	3.125 $\times 10^{2}$	2.290 $\times 10^{1}$
	40	-1.413 ± 10.40 i	1.280	7.320 $\times 10^{-2}$
	80	-1.411 ± 10.40 i	1.345 $\times 10^{-4}$	1.484 $\times 10^{-5}$
	160	-1.411 ± 10.40 i	1.346 $\times 10^{-4}$	1.484 $\times 10^{-5}$
1000				
	20	-1.225 ± 11.55 i	3.829 $\times 10^{2}$	3.558 $\times 10^{1}$
	40	-1.413 ± 10.40 i	2.842	1.259 $\times 10^{-1}$
	80	-1.411 ± 10.40 i	8.048 $\times 10^{-5}$	9.161 $\times 10^{-6}$
	160	-1.411 ± 10.40 i	8.048 $\times 10^{-5}$	9.161 $\times 10^{-6}$
2000				
	20	-2.282 ± 10.34 i	1.352 $\times 10^{2}$	8.241
	40	-1.377 ± 10.32 i	3.357 $\times 10^{1}$	1.865
	80	-1.411 ± 10.40 i	2.484 $\times 10^{-3}$	7.816 $\times 10^{-5}$
	160	-1.411 ± 10.40 i	6.275 $\times 10^{-5}$	6.018 $\times 10^{-6}$
4000				
	20	-1.875 ± 10.08 i	4.221 $\times 10^{2}$	1.241 $\times 10^{1}$
	40	-2.033 ± 10.01 i	8.613 $\times 10^{1}$	3.635
	80	-1.396 ± 10.39 i	5.660	1.513 $\times 10^{-1}$
	160	-1.411 ± 10.40 i	6.500 $\times 10^{-5}$	7.915 $\times 10^{-6}$

TABLE 15
The effect of Arnoldi size and Cayley parameters on the problem of stability of a heated plume. These results are for the most unstable eigenvalue at $Gr = 1. \times 10^9$, and for the 160 × 320 grid.

$\sigma = -\mu$	Arnoldi Size	Eigenvalue (normalized by 10^{-1})	Direct Residual	Rayleigh Quotient
250				
	20	14.43 ± 112.1 i	1.078 $\times 10^{3}$	7.801 $\times 10^{2}$
	40	-0.3819 ± 111.3 i	9.870 $\times 10^{2}$	4.349 $\times 10^{2}$
	80	-1.525 ± 110.9 i	64.57	3.614 $\times 10^{-1}$
	160	-1.425 ± 111.0 i	1.009 $\times 10^{-2}$	2.330 $\times 10^{-4}$
500				
	20	6.043 ± 109.8 i	9.801 $\times 10^{2}$	2.678 $\times 10^{2}$
	40	-1.105 ± 110.1 i	4.317 $\times 10^{2}$	1.733 $\times 10^{1}$
	80	-1.425 ± 110.9 i	3.090 $\times 10^{-1}$	6.630 $\times 10^{-4}$
	160	-1.425 ± 111.0 i	3.400 $\times 10^{-3}$	1.232 $\times 10^{-4}$
1000				
	20	0.5203 ± 112.8 i	8.773 $\times 10^{2}$	8.723 $\times 10^{1}$
	40	-1.354 ± 110.8 i	73.40	4.458 $\times 10^{-1}$
	80	-1.425 ± 111.0 i	1.750 $\times 10^{-2}$	3.309 $\times 10^{-4}$
	160	-1.425 ± 111.0 i	3.373 $\times 10^{-3}$	3.231 $\times 10^{-4}$
2000				
	20	5.136 ± 116.7 i	6.654 $\times 10^{2}$	3.066 $\times 10^{1}$
	40	-1.824 ± 111.0 i	1.245 $\times 10^{2}$	2.779
	80	-1.424 ± 111.0 i	1.492 $\times 10^{-1}$	4.795 $\times 10^{-4}$
	160	-1.425 ± 111.0 i	1.468 $\times 10^{-3}$	6.247 $\times 10^{-5}$
4000				
	20	1.332 ± 156.8 i	1.508 $\times 10^{3}$	3.168 $\times 10^{2}$
	40	2.827 ± 106.8 i	6.403 $\times 10^{2}$	19.14
	80	-1.376 ± 110.9 i	11.03	5.097 $\times 10^{-2}$
	160	-1.425 ± 111.0 i	1.428 $\times 10^{-3}$	1.037 $\times 10^{-4}$

10. CONCLUSIONS

We have demonstrated both the capabilities and the limitations of using a general purpose finite element code and eigensolver for fluid stability calculations. We validated and verified this approach on a wide variety of thermal convection problems ranging from the Classical Rayleigh-Bénard problem to the onset of oscillatory convection in roll patterns, and the instability of a heated plume. Due to the size of the problems involved it was necessary to use iterative methods for the linear algebraic calculations. The largest problem we solved had over 16 million unknowns. We believe that the problems presented are impressive because of the three dimensional problems and the highly advective problems. Some of these problems were chosen to push the limits of the techniques presented in this paper. None of these problems indicated that the techniques had reached any inherent limitation.

We carefully analyzed our results by starting with relatively simple problems that can be compared to semi-analytical results. The code was shown to give excellent

agreement with the semi-analytical results. We have also presented results where no semi-analytical results are available but we validated against existing results attained by traditional transient based methods and verified by examining the rate of convergence of the discrete eigenvalues as the mesh was refined.

Our results show that the accuracy of the calculations deteriorates as the flow is advectively dominated. However, our results demonstrate that this is not a problem with the eigensolver but with whether the discretization is sufficiently resolved. Thus, the use of transient based methods would encounter the same difficulties. We maintain that our results are as reliable as those obtained using transient integration, but that our results are more efficiently computed because we use a Krylov subspace method instead of the power method, and because we use a frozen Jacobian. We believe that our use of preconditioned Krylov iterative methods were successful because of the high quality and robust implementation of these algorithms, ARPACK, and Aztec.

APPENDIX A

Eigenvalues for the Classical and Rotating Rayleigh-Bénard Problem

In this appendix we discuss how we use separation of variables to reduce the two and three dimensional Rayleigh-Bénard eigenvalue problems to one dimensional eigenvalue problems that can be solved using a spectral collocation method.

A.1. THE TWO DIMENSIONAL RAYLEIGH-BÉNARD PROBLEM

We present the analysis of the stability of the no-flow solution to the two dimensional Rayleigh-Bénard problem in a box (Section 5.1). The stability of this solution is determined by the eigenvalue problem

$$\sigma \mathbf{u} + \frac{1}{\rho}\nabla p = \nu \nabla^2 \mathbf{u} + g\beta T \mathbf{e}_z \tag{A.1a}$$

$$\sigma T - w\frac{\Delta T}{H} = \kappa \nabla^2 T \tag{A.1b}$$

$$\nabla \cdot \mathbf{u} = 0 \tag{A.1c}$$

$$\mathbf{u}(x,0) = \mathbf{u}(x,H) = 0 \tag{A.1a}$$

$$T(x,0) = T(x,H) = 0 \tag{A.1b}$$

$$\frac{\partial}{\partial x}T(0,z) = \frac{\partial}{\partial x}T(L,z) = 0 \tag{A.2}$$

$$u(0,z) = u(L,z) = 0 \tag{A.3}$$

$$\frac{\partial}{\partial x}w(0,z) = \frac{\partial}{\partial x}w(L,z) = 0. \tag{A.4}$$

This eigenvalue problem can be solved using separation of variables. We assume our solutions are of the form

$$\sigma = \frac{\kappa}{H^2}\hat{\sigma},$$

$$u(x,z) = \sin(\hat{k}x/H)\frac{\kappa}{H}\hat{u}(\hat{z})$$

$$w(x,z) = \cos(\hat{k}x/H)\frac{\kappa}{H}\hat{w}(\hat{z})$$

$$T(x,z) = \cos(\hat{k}x/H)\Delta T\hat{T}(\hat{z})$$

$$p(x,z) = \cos(\hat{k}x/H)\frac{\rho\kappa^2}{H^2}\hat{p}(\hat{z})$$

$$\hat{z} = z/H.$$

Solutions of this form will satisfy the vertical boundary conditions provided $\hat{k}$ takes on the discrete set of values

$$\hat{k}_m = \frac{\pi m H}{L} \quad , \quad m = 0, \pm 1, \pm 2, \pm 3...$$

In order to satisfy our two dimensional eigenvalue problem it is now only necessary that the functions $(\hat{u}, \hat{w}, \hat{T}, \hat{p})$ satisfy the one dimensional eigenvalue problem

$$\hat{\sigma}\hat{u} - \hat{k}_m\hat{p} = Pr(\hat{u}'' - \hat{k}_m^2\hat{u}) \tag{A.5}$$

$$\hat{\sigma}\hat{w} + \hat{p}' = Pr(\hat{w}'' - \hat{k}_m^2\hat{w}) + RaPrT \tag{A.6}$$

$$\hat{\sigma}\hat{T} - \hat{w} = \hat{T}'' - \hat{k}_m^2\hat{T} \tag{A.7}$$

$$-\hat{k}_m\hat{u} + \hat{w}' = 0 \tag{A.8}$$

where the primes refer to differentiation with respect to $\hat{z}$,

$$Ra = \frac{g\beta H^3\Delta T}{\kappa\nu}$$

is the dimensionless Rayleigh number and

$$Pr = \frac{\nu}{\kappa}$$

is the dimensionless Prandtl number, and the boundary conditions are

$$\hat{u}(0) = \hat{u}(1) = \hat{w}(0) = \hat{w}(1) = \hat{T}(0) = \hat{T}(1) = 0. \tag{A.9}$$

In order to get the eigenvalues with the largest real part of the two dimensional eigenvalue problem, we need to compute the eigenvalues for $m = 0, 1, 2, \ldots$ and select the largest eigenvalues from these. Assuming we only want the first four largest eigenvalues, it is only necessary to compute the eigenvalues for small values of m.

We will not discuss the details of the spectral calculation, but state that these calculations were carried out with extreme precision and for our purposes can be considered to give exact answers.

A.2. THE THREE DIMENSIONAL RAYLEIGH-BÉNARD PROBLEM

We present the analysis of the stability of the no-flow solution to the three dimensional Rayleigh-Bénard problem in a box (Section 5.2). As in the case of the two dimensional Rayleigh-Bénard problem, the stability of this solution is determined by the equations A.1a–A.1c. Once again the boundary conditions on the horizontal walls require that both the velocity and the temperature vanish (Eqs. A.1a–A.1b). The boundary conditions on the vertical walls require that there is no normal velocity, no tangential stress, and no flux of heat:

$$u(x,y,z) = \frac{\partial v(x,y,z)}{\partial x} = \frac{\partial w(x,y,z)}{\partial x} = \frac{\partial T(x,y,z)}{\partial x} = 0 \text{ for } x = 0, L \quad \text{(A.10)}$$

$$v(x,y,z) = \frac{\partial u(x,y,z)}{\partial y} = \frac{\partial w(x,y,z)}{\partial y} = \frac{\partial T(x,y,z)}{\partial y} = 0 \text{ for } y = 0, W. \quad \text{(A.11)}$$

To solve the eigenvalue problem, we assume solutions of the form

$$\sigma = \frac{\kappa}{H^2}\hat{\sigma}$$

$$u(x,y,z) = \sin(\hat{k}_1 x/H)\cos(\hat{k}_2 y/H)\frac{\kappa}{H}\hat{u}(\hat{z})$$

$$v(x,y,z) = \cos(\hat{k}_1 x/H)\sin(\hat{k}_2 y/H)\frac{\kappa}{H}\hat{v}(\hat{z})$$

$$w(x,y,z) = \cos(\hat{k}_1 x/H)\cos(\hat{k}_2 y/H)\frac{\kappa}{H}\hat{w}(tz)$$

$$T(x,y,z) = \cos(\hat{k}_1 x/H)\cos(\hat{k}_2 y/H)\Delta T\hat{T}(\hat{z})$$

$$p(x,y,z) = \cos(\hat{k}_1 x/H)\cos(\hat{k}_2 y/H)\frac{\rho\kappa^2}{H^2}\hat{p}(\hat{z})$$

$$\hat{z} = z/H.$$

Solutions of this form will be eigenvectors of our stability equations provided

$$\hat{k}_1 = m\pi H/L \quad m = 0, \pm 1, \pm 2, \pm 3 \ldots$$

$$\hat{k}_2 = n\pi H/W \quad m = 0, \pm 1, \pm 2, \pm 3 \ldots$$

and provided the functions $\hat{u}$,$\hat{v}$, $\hat{w}$, $\hat{p}$, and $\hat{T}$ satisfy the one dimensional eigenvalue problem

$$\hat{\sigma}\hat{u} - \hat{k}_1\hat{p} = Pr(\hat{u}'' - \hat{k}^2\hat{u}) \quad \text{(A.12)}$$

$$\hat{\sigma}\hat{v} - \hat{k}_2\hat{p} = Pr(\hat{v}'' - \hat{k}^2\hat{v}) \quad \text{(A.13)}$$

$$\hat{\sigma}\hat{w} + \hat{p}' = Pr(\hat{w}'' - \hat{k}^2\hat{w}) + RaPr\hat{T} \quad \text{(A.14)}$$

$$\hat{\sigma}\hat{T} - \hat{w} = \hat{T}'' - \hat{k}^2\hat{T} \tag{A.15}$$

$$-\hat{k}_1\hat{u} - \hat{k}_2\hat{v} + \hat{w}' = 0 \tag{A.16}$$

$$\hat{k}^2 = \hat{k}_1^2 + \hat{k}_2^2$$

along with the boundary conditions,

$$\hat{u}(z) = \hat{v}(z) = \hat{w}(z) = 0 \text{ for } z = 0, 1 \tag{A.17}$$

and

$$\hat{T}(z) = 0 \text{ for } z = 0, 1. \tag{A.18}$$

In order to compute the largest eigenvalues of the three dimensional problem we need to compute the largest eigenvalues for m and n; since we are only interested in the 4 largest eigenvalues we only need to use small values of m and n. Once again, the one dimensional eigenvalue problem was solved using a spectral collocation method and for our purposes can be considered to give exact answers.

A.3. EIGENVALUES FOR THE ROTATING RAYLEIGH-BÉNARD PROBLEM

Here we show how to reduce the eigenvalues for the rotating Rayleigh-Bénard problem (Section 5.3) to a one dimensional eigenvalue problem. The stability (assuming axisymmetric disturbances) of the state of uniform rotation is governed by the eigenvalue problem

$$\sigma u - 2\Omega v + \frac{1}{\rho}\frac{\partial p}{\partial r} = \nu\nabla^2 u$$

$$\sigma v + 2\Omega u = \nu\nabla^2 v$$

$$\sigma w + \frac{1}{\rho}\frac{\partial p}{\partial z} = \nu\nabla^2 w + g\beta T$$

$$\sigma T - \frac{\Delta T}{H}w = \kappa\nabla^2 T$$

$$\frac{1}{r}\frac{\partial}{\partial r}(ru) + \frac{\partial w}{\partial z} = 0.$$

We also impose the boundary conditions

$$u(r, z) = v(r, z) = \frac{\partial w(r, z)}{\partial r} = \frac{\partial T(r, z)}{\partial r} = 0 \text{ for } r = R$$

and

$$\mathbf{u}(r, z) = T(r, z) = 0 \text{ for } z = 0, H.$$

We solve this eigenvalue problem using separation of variables. To use separation of variables we assume that our eigenfunctions have the form

$$\sigma = \frac{\kappa}{H^2}\hat{\sigma}$$

$$u(r,z) = \hat{u}(\hat{z})\frac{\kappa}{H}J_1(\hat{k}r/H)$$

$$v(r,z) = \hat{v}(\hat{z})\frac{\kappa}{H}J_1(\hat{k}r/H)$$

$$w(r,z) = \hat{w}(\hat{z})\frac{\kappa}{H}J_0(\hat{k}r/H)$$

$$T(r,z) = \hat{T}(\hat{z})\Delta T J_0(\hat{k}r/H)$$

$$p(r,z) = \hat{p}(\hat{z})\frac{\rho\kappa^2}{H^2}J_0(\hat{k}r/H)$$

$$\hat{z} = z/H$$

where $\hat{k}$ is restricted to

$$\hat{k}_m = \frac{\gamma_m H}{R}$$

where γ_m is the mth zero of the function $J_1(z)$. Since $J_0'(z) = -J_1(z)$, this restriction on $\hat{k}$ guarantees that the boundary conditions on the side walls will be satisfied. In addition, the functions $\hat{u}$, $\hat{v}$, $\hat{w}$, $\hat{T}$ and $\hat{p}$ must satisfy the one dimensional eigenvalue problem:

$$\hat{\sigma}\hat{u} - \hat{k}\hat{p} = Pr(\hat{u}'' - \hat{k}^2\hat{u}) + Pr\epsilon^2\sqrt{Ta}\hat{v}$$

$$\hat{\sigma}\hat{v} = Pr(\hat{v}'' - \hat{k}^2\hat{v}) - Pr\epsilon^2\sqrt{Ta}\hat{u}$$

$$\hat{\sigma}\hat{w} + \hat{p}' = Pr(\hat{w}'' - \hat{k}^2\hat{w}) + RaPr\hat{T}$$

$$\hat{\sigma}\hat{T} - \hat{w} = \hat{T}'' - \hat{k}^2\hat{T}$$

$$-\hat{k}\hat{u} + \hat{w}' = 0$$

along with the boundary conditions

$$\hat{u}(z) = \hat{v}(z) = \hat{w}(z) = \hat{T}(z) = 0 \text{ for } \hat{z} = 0, H$$

where

$$Ra = \frac{g\beta\Delta T H^3}{\kappa\nu}$$

$$Ta = \frac{4\Omega^2 R^4}{\nu^2}$$

and

$$\epsilon = \frac{H}{R}.$$

Once again this problem was solved using a spectral collocation code, and we found the largest eigenvalues from among the modes given by $m = 0, \pm 1, \pm 2, \ldots$.

APPENDIX B

Eigenvalues for Convection In a Porous Medium

In this appendix we show how to analyze the stability of the steady state solution

$$T = T_{ref} - \Delta T(z - H)/H$$

$$\mathbf{u}_{av} = 0$$

to the equations for convection in a porous medium.

In the Hele-Shaw approximation, the stability of this solution is governed by the eigenvalues σ of the eigensystem

$$\nabla^2 p = \rho g \beta \frac{\partial T}{\partial z}$$

$$\sigma T - w_{av} \frac{\Delta T}{H} = \kappa \nabla^2 T$$

$$\mathbf{u}_{av} = \frac{k}{\mu} (\nabla p - \rho g \beta T \mathbf{e}_z)$$

along with the boundary conditions

$$T(x, 0) = T(x, H) = 0$$

$$\frac{\partial T}{\partial x}(x, z) = 0 \text{ for } x = 0, L$$

$$\nabla \cdot p = 0 \ \textit{on all boundaries.}$$

We can analyze this eigenvalue problem by assuming that the eigenvalues and eigenfunctions have the form

$$\sigma = \frac{\kappa}{H^2} \hat{\sigma}$$

$$p(x, z) = \hat{p}(\hat{z}) \rho g \beta \Delta T H \cos(\hat{k}_m x / H)$$

$$T(x, z) = \hat{T}(\hat{z}) \Delta T \cos(\hat{k}_m x / H)$$

$$\hat{z} = z / H$$

where $\hat{k}_m$ must take on the discrete values

$$\hat{k}_m = \frac{m \pi H}{L}$$

and $\hat{p}$ and $\hat{T}$ satisfy the one dimensional eigenvalue problem

$$\hat{p}'' - \hat{k}_m^2 \hat{p} - \hat{T}' = 0 \tag{B.1}$$

$$\hat{T}'' - \hat{k}_m^2 \hat{T} = -Ra_{HS}(\hat{p}' - \hat{T}) + \hat{\sigma}\hat{T} \tag{B.2}$$

$$\hat{p}'(z) = \hat{T}(z) = 0 \;\; at \;\; \hat{z} = 0, 1 \tag{B.3}$$

where

$$Ra_{HS} = \frac{g\beta\Delta T k H}{\nu\kappa} = \frac{g\beta\Delta T H W^2}{12\kappa\nu}. \tag{B.4}$$

This one dimensional eigenvalue problem is once again solved using a spectral collocation code, and the largest eigenvalues are found by searching through small values of m.

APPENDIX C

The Eigenvalues for a Thermo-Siphon

We now present an asymptotic analysis that is used to check the numerical results for the stability of the state of rest in a thermo-siphon.

We assume that the radius R_T of the tube is small compared to the radius of the hoop R_H. This allows us to make the approximation that the flow is always unidirectional, in the direction tangent to the midline of the hoop. That is, in our cylindrical coordinate system $u = w = 0$. Continuity now requires that $v(r, z, \theta)$ is independent of θ. Because the hoop is circular, we take the gravity vector $\mathbf{g} = g\sin(\theta)\mathbf{e}_\theta$. We multiply the energy equation by $\sin(\theta)$ and integrate from $-\pi$ to π, do the same but multiply by $\cos(\theta)$, and integrate the azimuthal momentum equation from $-\pi$ to π to get the approximate equations

$$Pr\frac{\partial\tilde{\Phi}}{\partial\tilde{t}} - \lambda\tilde{\Psi}\tilde{v} = \tilde{\nabla}^2\tilde{\Phi} \tag{C.1}$$

$$Pr\frac{\partial\tilde{\Psi}}{\partial\tilde{t}} + \lambda\tilde{\Phi}\tilde{v} = \tilde{\nabla}^2\tilde{\Psi} \tag{C.2}$$

$$\frac{\partial\tilde{v}}{\partial\tilde{t}} - \tilde{\nabla}^2\tilde{v} = \tilde{\Phi} \tag{C.3}$$

and the boundary conditions

$$\tilde{v}(\hat{x}, \hat{y}) = 0 \text{ on boundary} \tag{C.4}$$

$$\tilde{\Phi}(\hat{x}, \hat{y}) = \frac{B}{A} \text{ on boundary} \tag{C.5}$$

$$\tilde{\Psi}(\hat{x}, \hat{y}) = 1 \text{ on boundary} \tag{C.6}$$

where we have the parameters the diffusion ratio (Prandtl number) (C.7) and the control parameter (Rayleigh number) (C.8):

$$Pr = \frac{\nu}{\kappa}\,, \tag{C.7}$$

$$Ra_{therm} = \frac{g\beta R_T^4 A}{\kappa\nu R_H}\,, \tag{C.8}$$

where

$$\tilde{v}(\hat{x},\hat{y},\hat{t}) = \frac{\nu}{g\beta A R_T^2} v(r,z,\theta,t) \tag{C.9}$$

$$\tilde{\Phi}(\hat{x},\hat{y},\hat{t}) = \frac{1}{2\pi A}\int_{-\pi}^{\pi} \sin(\theta) T(r,z,\theta) d\theta \tag{C.10}$$

$$\tilde{\Psi}(\hat{x},\hat{y},\hat{t}) = \frac{1}{2\pi A}\int_{-\pi}^{\pi} \cos(\theta) T(r,z,\theta) d\theta \tag{C.11}$$

$$A = \frac{\Delta T}{2\pi}\int_{-\pi}^{\pi} f(\theta)\cos(\theta) d\theta \tag{C.12}$$

$$B = \frac{\Delta T}{2\pi}\int_{-\pi}^{\pi} f(\theta)\sin(\theta) d\theta \tag{C.13}$$

and

$$\hat{x} = (r - R_H)/R_T \tag{C.14}$$

$$\hat{y} = z/R_T \tag{C.15}$$

$$\hat{t} = \frac{\nu}{R_T^2} t. \tag{C.16}$$

The Laplacian in these equations is the two dimensional Laplacian in the variables $\hat{x}$ and $\hat{y}$. If we assume that our cross section is circular, and we introduce polar coordinates

$$\xi = \sqrt{\hat{x}^2 + \hat{y}^2} \tag{C.17}$$

these equations reduce to one dimensional partial differential equations:

$$Pr\frac{\partial\tilde{\Phi}}{\partial\tilde{t}} - Ra_{therm}\tilde{\Psi}\tilde{v} = \frac{1}{\xi}\frac{\partial}{\partial\xi}\left(\xi\frac{\partial\tilde{\Phi}}{\partial\xi}\right) \tag{C.18}$$

$$Pr\frac{\partial\tilde{\Psi}}{\partial\tilde{t}} + Ra_{therm}\tilde{\Phi}\tilde{v} = \frac{1}{\xi}\frac{\partial}{\partial\xi}\left(\xi\frac{\partial\tilde{\Psi}}{\partial\xi}\right) \tag{C.19}$$

$$\frac{\partial\tilde{v}}{\partial\tilde{t}} - \tilde{\nabla}^2\tilde{v} = \tilde{\Phi}. \tag{C.20}$$

For symmetric heating we have $B = 0$. In this case we always have the steady state solution $\tilde{\Phi} = 0$, $\tilde{\Psi} = 1$. Note that this is an asymptotic result; the full solution to the equations of motion has a small (symmetric) movement of fluid. We can analyze the stability of this steady solution to the asymptotic equations.

Carrying out a linearized stability analysis we get the eigenvalue problem

$$\sigma Pr\Psi = \nabla^2\Psi \tag{C.21}$$

$$\sigma \begin{pmatrix} Pr\Psi \\ v \end{pmatrix} = \nabla^2 \begin{pmatrix} \Phi \\ v \end{pmatrix} + \begin{pmatrix} v \\ \Phi \end{pmatrix} \tag{C.22}$$

$$\Phi(1) = \Psi(1) = w(1) = 0. \tag{C.23}$$

The critical value of the parameter Ra_{therm} where the solution goes unstable can be found analytically. It is given by

$$Ra_{therm_c} = s^4 \tag{C.24}$$

where s is the first zero of the zero order Bessel function J_0. Away from the critical value, we can compute the eigenvalues of this reduced system accurately using a spectral method.

APPENDIX D
The Eigenvalues for a Tilted Two or Three Dimensional Box

D.1. THE EIGENVALUES OF THE TILTED TWO DIMENSIONAL BOX

We discuss the eigenvalue problem associated with the tilted two dimensional box. The eigenvalue problem associated with the solution discussed in (6.2) is

$$\sigma u + u_0 \frac{\partial u}{\partial x} + w \frac{\partial u_0}{\partial z} + \frac{1}{\rho}\frac{\partial p}{\partial x} = \nu \nabla^2 u - g\beta \sin(\theta) T \tag{D.1a}$$

$$\sigma w + u_0 \frac{\partial w}{\partial x} + \frac{1}{\rho}\frac{\partial p}{\partial z} = \nu \nabla^2 w + g\beta \cos(\theta) T \tag{D.1b}$$

$$\sigma T + u_0 \frac{\partial T}{\partial x} + w \frac{\partial T_0}{\partial z} = \kappa \nabla^2 T \tag{D.1c}$$

$$\frac{\partial u}{\partial x} + \frac{\partial w}{\partial z} = 0 \tag{D.1d}$$

where u_0 and T_0 are given by 27a–27d.

We also impose the boundary conditions

$$\mathbf{u}(x,z) = T(x,z) = 0 \text{ for } z = \pm H/2 \tag{D.2}$$

$$T(0,z) - T(L,z) = \mathbf{u}(0,z) - \mathbf{u}(L,z) = p(0,z) - p(L,z) = 0. \tag{D.3}$$

We can reduce this to a one dimensional eigenvalue problem by assuming the solutions are of the form

$$\sigma = \frac{\kappa}{H^2}\hat{\sigma}$$

$$u(x,z) = e^{i\hat{k}x/H}\frac{\kappa}{H}\hat{u}(\hat{z})$$

$$w(x,z) = e^{i\hat{k}x/H}\frac{\kappa}{H}\hat{w}(\hat{z})$$

$$T(x,z) = e^{i\hat{k}x/H}\Delta T\hat{T}(\hat{z})$$

$$p(x,z) = e^{i\hat{k}x/H}\frac{\rho\kappa^2}{H^2}\hat{p}(\hat{z})$$

$$\hat{z} = z/H.$$

Assuming that $\hat{k}$ takes on the discrete values

$$\hat{k}_m = 2m\pi\frac{H}{L} \quad m = 0, 1, 2, 3...$$

the periodic boundary conditions will be satisfied. It is then only necessary that the functions $\hat{u}$, $\hat{w}$, $\hat{p}$, and $\hat{T}$ satisfy the one dimensional eigenvalue problem:

$$\hat{\sigma}\hat{u} - Pei\hat{k}_m f(\hat{z})\hat{u} - Pe\hat{w}\frac{df}{d\hat{z}} + i\hat{k}_m\hat{p} = Pr(\hat{u}'' - \hat{k}_m^2\hat{u}) - RaPr\sin(\theta)T \quad \text{(D.4)}$$

$$\hat{\sigma}\hat{w} - Pei\hat{k}_m f(\hat{z})\hat{w} + \hat{p}' = Pr(\hat{w}'' - \hat{k}_m^2\hat{w}) + RaPr\cos(\theta)T \quad \text{(D.5)}$$

$$\hat{\sigma}\hat{T} - iPe\hat{k}_m f(\hat{z})T - \hat{w} = \hat{T}'' - \hat{k}_m^2\hat{T} \quad \text{(D.6)}$$

$$i\hat{k}_m\hat{u} + \hat{w}' = 0 \quad \text{(D.7)}$$

along with the boundary conditions

$$\hat{u}(\pm 1/2) = \hat{w}(\pm 1/2) = \hat{T}(\pm 1/2) = 0. \quad \text{(D.8)}$$

Here

$$Pe = Ra\sin(\theta) \quad \text{(D.9)}$$

and

$$f(\hat{z}) = \frac{\hat{z}^3}{6} - \frac{\hat{z}}{24}. \quad \text{(D.10)}$$

We solve the eigenvalue problem using a spectral collocation method for $m = 0, 1, 2, \ldots$ and choose the 4 most unstable eigenvalues from these.

D.2. THE EIGENVALUES OF THE TILTED THREE DIMENSIONAL BOX

We consider the eigenvalue problem arising from the tilted three dimensional box discussed in section 6.3. In general it is not possible to find the eigenvalues of this problem using separation of variables. However, it is possible to use separation of variables for eigenfunctions that have no x velocity component and no x dependence, or that have no y velocity component or y dependence.

If a mode has no x velocity or x dependence the advection terms in the stability equations disappear, and we get the same eigenvalue problem as for the classical Rayleigh-Bénard problem, except that the Rayleigh number is replaced by $Ra\cos(\theta)$.

When there is no y velocity component or y dependence in the eigenfunction the eigenvalue problem is identical to the one for the tilted two dimensional box.

ACKNOWLEDGMENTS

The authors would like to acknowledge the support obtained from many members of the MP-Salsa and Aztec teams, including David Day, Karen Devine, Sudip Dosanjh, Gary Hennigan, Scott Hutchinson, Roger Pawlowski, John Shadid, Ray Tuminaro, and David Womble. We also thank Evangelos Coutsias of the University of New Mexico. This work was partially funded by the Accelerated Strategic Computing Initiative and the Mathematical, Information, and Computational Sciences programs at Sandia National Laboratories.

REFERENCES

1. W. E. Arnoldi. The principle of minimized iterations in the solution of the matrix eigenvalue problem. *Quart. J. Applied Mathematics*, 9:17–29, 1951.
2. F. H. Busse and R. M. Clever. Instabilities of convection rolls of moderate Prandtl number. *Journal of Fluid Mechanics*, 91(2):319–335, 1979.
3. S. Chandrasekhar. *Hydrodynamic and Hydromagnetic Stability*. Dover, 1970.
4. K. N. Christodoulou and L. E. Scriven. Finding leading modes of a viscous free surface flow: An asymmetric generalized eigenproblem. *Journal of Scientific Computing*, 3:355–406, 1988.
5. R. M. Clever and F. H. Busse. Convection rolls and their instabilities in the presence of a nearly insulating upper boundary. *Physics of Fluids*, 7(1):92–97, 1995.
6. K. A. Cliffe. Numerical calculations of the primary flow exchange process in the Taylor problem. *Journal of Fluid Mechanics*, 197:57–79, 1988.
7. K. A. Cliffe, T. J. Garratt, and A. Spence. Eigenvalues of the discretized Navier-Stokes equation with application to the detection of Hopf bifurcations. *Advances in Computational Mathematics*, 1:337–356, 1993.
8. K.A. Cliffe, A. Spence, and S.J. Tanvener. *The numerical analysis of bifurcation with application to fluid mechanics*, pages 39–131. Acta Numerica(2000). Cambridge University Press, 2000.
9. S. M. Cox and P. C. Matthews. Instability of rotating convection. *Journal of Fluid Mechanics*, 403:153–172, 2000.
10. P. G. Drazin and W. H. Reid. *Hydrodynamic Stability*. Cambridge University Press, New York, 1981.
11. W.S. Edwards, L.S. Tuckerman, R.A. Friesner, and D.C. Sorensen. Krylov methods for the incompressible Navier-Stokes equations. *Journal of Computational Physics*, 110(1):82–102, January 1994.
12. A. Fortin, M. Jardak, J.J. Gervais, and R. Pierre. Localization of Hopf bifurcations in fluid flow problems. *Int. J. Numer Methods Fluids*, 24:1185–1210, 1997.
13. D. Gottlieb and S. A. Orszag. *Numerical Analysis of Spectral Methods: Theory and Applications*. SIAM, Philadelphia, 1977.
14. B. Hendrickson and R. Leland. The Chaco user's guide: Version 2.0. Technical Report SAND94–2692, Sandia National Labs, Albuquerque, NM, June 1995.
15. R. A. W. M. Henkes and P. Le Quéré. Three-dimensional transition of natural-convection flows. *Journal of Fluid Mechanics*, 319:281–303, 1996.
16. J. R. Hughes, L. P. Franca, and G. M. Hulbert. A new finite element formulation for computational fluid dynamics: VIII. the Galerkin/least-squares method for advective-diffusive equations. *Comp. Meth. App. Mech. and Eng.*, 73:173–189, 1989.
17. R. J. A. Janssen and R. A. W. M. Henkes. Influence of Prandtl number on instability mechanisms and transition in a differentially heated square cavity. *Journal of Fluid Mechanics*, 290:319–344, 1995.
18. D. D. Joseph. *Stability of Fluid Motions*. Springer-Verlag, Berlin, 1976.
19. H. S. Kwak and J. M. Hyun. Natural convection in an enclosure having a vertical sidewall with time-varying temperature. *Journal of Fluid Mechanics*, 329:65–88, 1996.
20. R. B. Lehoucq, D. C. Sorensen, and C. Yang. *ARPACK USERS GUIDE: Solution of Large Scale Eigenvalue Problems with Implicitly Restarted Arnoldi Methods*. SIAM, Phildelphia, PA, 1998.

21. R.B. Lehoucq and A.G. Salinger. Large-scale eigenvalue calculations for stability analysis of steady flows on massively parallel computers. Technical Report 99-1593J, Sandia National Laboratories, Albuquerque, NM (USA), 1999. Accepted for publication in Int. J. Numer Methods Fluids.

22. C. C. Lin. *The Theory of Hydrodynamic Stability.* Cambridge University Press, 1955.

23. K. J. Maschhoff and D. C. Sorensen. P_ARPACK: An efficient portable large scale eigenvalue package for distributed memory parallel architectures. In Jerzy Wasniewski, Jack Dongarra, Kaj Madsen, and Dorte Olesen, editors, *Applied Parallel Computing in Industrial Problems and Optimization*, volume 1184 of *Lecture Notes in Computer Science*, Berlin, 1996. Springer–Verlag.

24. Karl Meerbergen and Alastair Spence. Implicitly restarted Arnoldi with purification for the shift–invert transformation. *Mathematics of Computation*, 218:667–689, 1997.

25. H.D. Mittelmann, K.-T. Chang, D.F. Jankowski, and G.P. Neitzel. Iterative solution of the eigenvalue problem in Hopf bifurcation for the Boussinesq equations. *SIAM J. Scientific Computing*, 15(3):704–712, May 1994.

26. M. Morzyński, K. Afanasiev, and F. Thiele. Solution of the eigenvalue problems resulting from global non-parallel flow stability analysis. *Computer Methods in Applied Mechanics and Engineering*, 169:161–176.

27. Y. Nakamura. Spatio-temporal dynamics of forced periodic flows in a confined domain. *Physics of Fluids*, 9(11):3275–3287, 1997.

28. S. Paolucci and D. R. Chenoweth. Transition to chaos in a differentially heated vertical cavity. *Journal of Fluid Mechanics*, 201:379–410, 1989.

29. P. Le Quéré and M. Behnia. From onset of unsteadiness to chaos in a differentially heated square cavity. *Journal of Fluid Mechanics*, 359:81–107, 1998.

30. R. N. Rudakov. Spectrum of perturbations and stability of convective motion between vertical plates. *Prikl Math Mekh*, 31:376, 1967.

31. H. Schlichting. *Boundary-Layer Theory.* McGraw-Hill, New York, 1979.

32. J.N. Shadid. A fully-coupled Newton-Krylov solution method for parallel unstructured finite element fluid flow, heat and mass transport. *IJCFD*, 12:199–211, 1999.

33. J.N. Shadid, R.S. Tuminaro, and H.F. Walker. An inexact Newton method for fully coupled solution of the Navier-Stokes equations with heat and mass transport. *Journal of Computational Physics*, 137:155–185, 1997.

34. Y. Sone, K. Aoki, and H. Sugimoto. The Bénard problem for a rarefied gas: Formation of steady flow patterns and stability of array of rolls. *Physics of Fluids*, 9(12):3898–3914, 1997.

35. A. V. Tangborn, S. Q. Zhang, and V. Lakshminarayanan. A three-dimensional instability in mixed convection with streamwise periodic heating. *Physics of Fluids*, 7(11):2648–2658, 1995.

36. K. E. Torrance and J. A. Rockett. Numerical study of natural convection in an enclosure with localized heating from below: Creeping flow to the onset of laminar instability. *Journal of Fluid Mechanics*, 36:33–54, 1969.

37. L. S. Tukerman, F. Bertagnolio, O. Daube, P. Le Quéré, and D. Barkley. Stokes preconditioning for the inverse Arnoldi method. In D. Henry and A. Bayeon, editors, *Notes on Numerical Fluid Mechanics*, volume 74, 2000.

38. R. S. Tuminaro, M.A. Heroux, S. A. Hutchinson, and J. N. Shadid. Aztec user's guide: Version 2.1. Technical Report SAND99-8801J, Sandia National Laboratories, Albuquerque, NM, 1999.

39. J.L.M. van Dorsselaer. Computing eigenvalues occuring in continuation methods with the Jacobi-Davidson QZ method. *Journal of Computational Physics*, 138(CP975844):714–733, 1997.

40. G. E. Willis and J. W. Deardorff. The oscillatory motions of Rayleigh convection. *Journal of Fluid Mechanics*, 44(4):661–672, 1970.

41. K. H. Winters. A bifurcation study of laminar flow in a curved tube of rectangular cross section. *Journal of Fluid Mechanics*, 180:343–369, 1987.

42. R. A. Wooding. Steady state free thermal convection of liquid in a saturated porous medium. *Journal of Fluid Mechanics*, 2:273–285, 1956.

43. S. Xin and P. Le Quéré. Direct numerical simulations of two-dimensional chaotic natural convection in a differentially heated cavity of aspect ratio 4. *Journal of Fluid Mechanics*, 304:87–118, 1995.

44. S. Xin, P. Le Quéré, and O. Daube. Natural convection in a differentially heated horizontal cylinder: Effects of Prandtl number on flow structure and instability. *Physics of Fluids*, 9(4):1014–1033, 1997.